ARTICLE

JNK regulates ciliogenesis through the interflagellar transport complex and actin networks

Maria Chatzifrangkeskou[1] , Panayiotis Kouis[2] , and Paris A. Skourides[1]

The c-Jun N-terminal kinase (JNK) regulates various important physiological processes. Although the JNK pathway has been under intense investigation for over 20 yr, its complexity is still perplexing, with multiple protein partners underlying the diversity of its activity. We show that JNK is associated with the basal bodies in both primary and motile cilia. Loss of JNK disrupts basal body migration and docking and leads to severe ciliogenesis defects. JNK's involvement in ciliogenesis stems from a dual role in the regulation of the actin networks of multiciliated cells (MCCs) and the establishment of the intraflagellar transport-B core complex. JNK signaling is also critical for the maintenance of the actin networks and ciliary function in mature MCCs. JNK is implicated in the development of diabetes, neurodegeneration, and liver disease, all of which have been linked to ciliary dysfunction. Our work uncovers a novel role of JNK in ciliogenesis and ciliary function that could have important implications for JNK's role in the disease.

Introduction

Motile cilia are microtubule-based protrusions, essential for the generation of directional fluid flow, which is critical for clearing mucus in the airways, transporting the egg through the oviduct, and circulating cerebrospinal fluid in the cerebral ventricles (Brooks and Wallingford, 2014; Spassky and Meunier, 2017; Boutin and Kodjabachian, 2019). In multiciliated cells (MCCs), modified centrioles (basal bodies) migrate and dock to the cell apical surface, a process that involves actin assembly (Boisvieux-Ulrich et al., 1990; Dawe et al., 2007). Additionally, accessory structures required for ciliogenesis are assembled on the basal bodies, followed by cilium elongation and ciliary beating (Wallingford, 2010; Zhang and Mitchell, 2015). At the ciliary base, there are two subregions: transition fibers (TF) and the transition zone (TZ). TFs form a nine-bladed propeller-like structure linking the basal body to the ciliary membrane (Wei et al., 2015). Above TF is the TZ that functions as a molecular gate and is characterized by the Y-links connecting axoneme microtubules to the ciliary membrane (Wei et al., 2015). Defects in motile cilia cause a wide range of disorders known as motile ciliopathies (Hyland and Brody, 2021). Despite major efforts, our understanding of ciliogenesis remains incomplete.

JNK belongs to the family of mitogen-activated protein kinases (MAPKs) and is activated by pleiotropic signals including environmental stresses, growth factors, and cytokines (Kyriakis and Avruch, 2001). JNK is encoded by three different genes: *JNK1*, *JNK2*, and *JNK3* and, similar to other MAP kinases, it

is activated by dual phosphorylation mediated by the mitogen-activated protein kinase kinase (MKKs), MKK4 and MKK7 (Yan et al., 1994; Tournier et al., 1997). Once activated, JNK phosphorylates and regulates the activity of transcription factors (e.g., Myc, c-Jun, and Elk1), actin-regulating proteins (Myristoylated Alanine-Rich C-kinase Substrate-Like protein 1 (MARCKSL1), cofilin-1, CapZIP, and smoothelin-like-2 protein), and microtubule-regulating proteins (MAP1B, MAP2, motor protein kinesin light chain; Morton et al., 2003; Eyers et al., 2005; Björkblom et al., 2012; Gordon et al., 2013; Slee and Lowe-Krentz, 2013; Komulainen et al., 2014; Ramkumar et al., 2018; Ishikawa et al., 2019; Benoit et al., 2021). JNK is involved in embryonic development and organogenesis in zebrafish, and the knockdown of JNK1 resulted in serious malformations of embryos (Xiao et al., 2013). Additionally, JNK is activated by Wnt5a stimulation to regulate convergent extension movements during gastrulation in *Xenopus* embryos (Yamanaka et al., 2002).

Here, we have identified a previously unreported role of JNK in ciliogenesis and ciliary function through the regulation of actin meshwork in MCCs. Intriguingly, JNK kinase activity appears to be essential for proper basal body migration and apical docking and multiciliation. In addition, we have constructed an airyscan super-resolution map of the transition zone and the transition fiber structures of motile cilia. The molecular maps we have built here will provide an ideal guide to future studies

---

[1]Department of Biological Sciences, University of Cyprus, Nicosia, Cyprus; [2]Respiratory Physiology Laboratory, Medical School, University of Cyprus, Nicosia, Cyprus.

Correspondence to Paris A. Skourides: skourip@ucy.ac.cy; Maria Chatzifrangkeskou: chatzifrangkeskou.maria@ucy.ac.cy.

that will enhance our understanding of the molecular basic ciliopathy syndromes.

Results

JNK is closely associated with the basal bodies (BBs) of both motile and primary cilia

Whole-mount immunostaining of *Xenopus* embryos at stage 30 with a previously characterized antibody raised against phosphorylated JNK (pJNK) and acetylated tubulin, a marker of cilia, produced a punctate pattern near the apical surface of *Xenopus* MCCs, reminiscent of basal bodies (Fig. 1 A). Higher magnification images demonstrated that pJNK is localized at the base of motile cilia (Fig. 1, B–B''). JNK inhibitor treatment of embryos led to the loss of pJNK signal from the basal bodies, confirming the specificity of the antibody staining (Fig. S1 A). Staining with polyclonal JNK antibodies that display cross reactivity in Western blotting with the frog protein gave poor staining and very high background (Fig. S1 B). To better examine the precise localization of the protein and enable live imaging of protein dynamics, we expressed exogenous GFP-JNK1 in *Xenopus* embryos. Embryos ventrally coinjected with GFP-JNK and RFP-centrin displayed a ring-shaped pattern of JNK around basal bodies (Fig. 1 C), which overlaps with pJNK staining (Fig. S1 C), while unconjugated GFP control exhibited a diffuse cytosolic pattern demonstrating that the association with the basal bodies is specific to JNK (Fig. S1 D). The above data suggest that JNK is closely associated with the basal bodies and the pJNK staining suggests that BB-associated JNK is specifically activated at these sites. To confirm the activation of BB-associated JNK, we used a previously characterized intramolecular FRET biosensor of JNK engineered to detect endogenous JNK activity, which has Citrine (acceptor), the phosphoamino acid binding domain FHA1 (forkhead associated domain 1) paired with a substrate sequence based on Jun dimerization protein 2 (JDP2) phosphorylation site, linked to the JDP2 docking domain and enhanced cyan fluorescent protein (ECFP; donor; Fosbrink et al., 2010). This sensor responds to the binding of JDP2 to the phosphoamino acid binding domain upon its phosphorylation by JNK leading to increased FRET. We thus injected the mRNA of the JNK biosensor into the ventral animal poles of four cell-stage embryos and recorded ECFP and citrine fluorescence using spectral imaging (lambda mode, λ scan). Quantification of the intensity of Citrine in relation to ECFP revealed higher ratios specifically at basal bodies, suggesting elevated FRET in these areas (Fig. S1 E). This is visualized in Fig. S1 E, where the YFP/CFP ratio is generated after processing and is presented color coded as previously described (Kardash et al., 2011). This confirms that JNK is specifically activated at the basal bodies in agreement with the phospho-specific antibody staining. Given the phosphorylation of BB-associated JNK, we then asked if this association depends on its kinase activity. However, we did not observe changes in the localization of GFP-JNK1 following treatment with a JNK-specific inhibitor, SP600125 (Fig. S1 F).

We subsequently explored the possibility that JNK is associated with the basal bodies in other cell types and other types of cilia. JNK was also found in association with the basal bodies of the motile monocilia in cells of the gastrocoel roof plate (GRP) and primary cilia of the neural tube (Fig. 1, D–E'). JNK was also localized at the basal bodies of primary cilia in HeLa cells after serum-starvation-induced ciliogenesis (Fig. 1 F). These findings suggest that JNK associates with the basal bodies in all types of cilia.
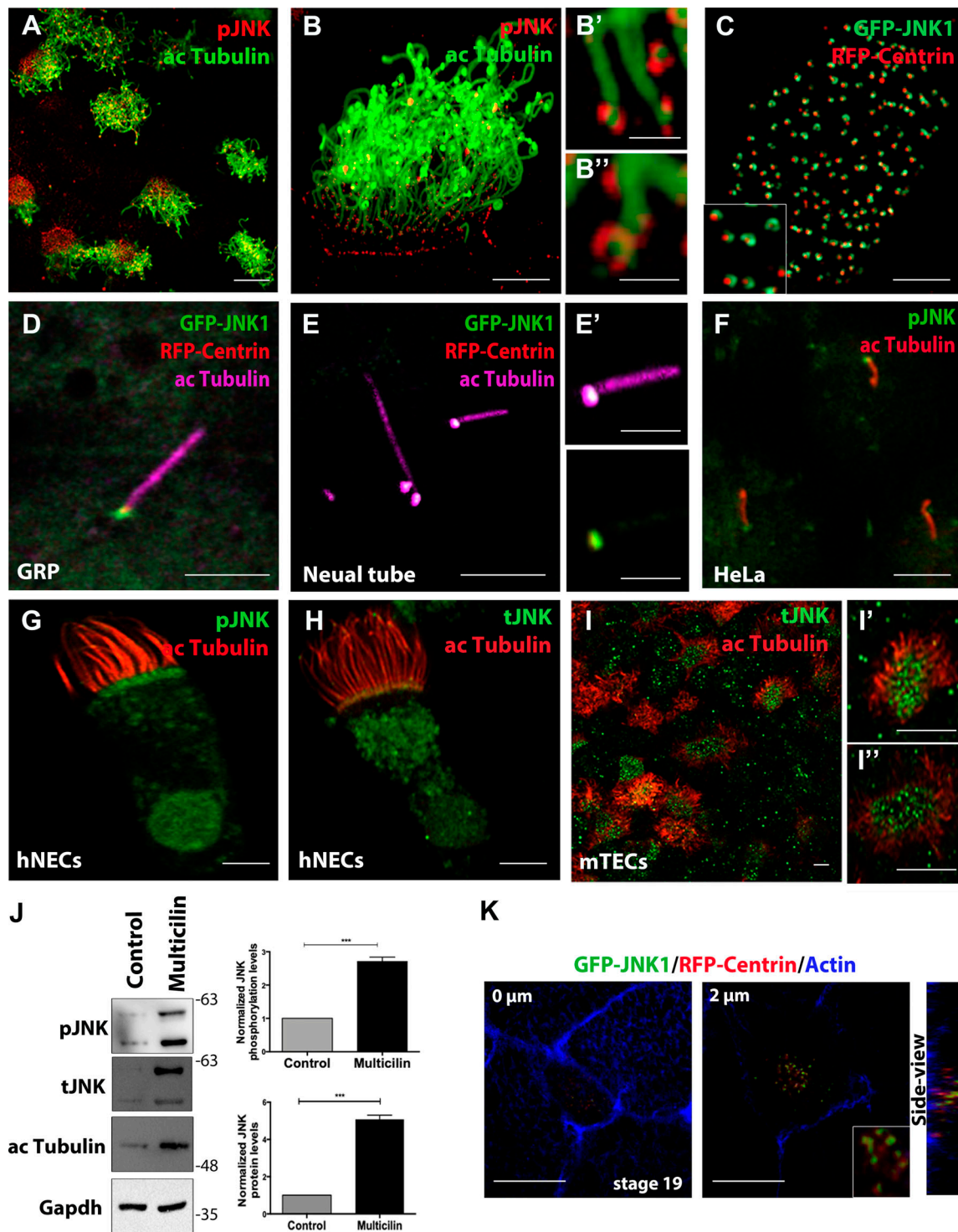
We next investigated whether the association of JNK with the basal bodies of MCCs is conserved in mammals. We thus carried out immunofluorescence staining using pJNK and tJNK-specific antibodies in human ciliated nasal epithelial cells obtained by transnasal brush biopsies from healthy volunteers. Costaining with acetylated tubulin revealed a punctate localization of phospho- and total-JNK protein at the base of ciliary axonemes in agreement with the *Xenopus* data (Fig. 1, G and H). We also exposed confluent human nasal cells to an air–liquid interface (ALI) to trigger ciliogenesis, further confirming that JNK was highly enriched at the apical surface of human MCCs (Fig. S1 G). A similar pattern was observed in the MCCs of mouse tracheas (Fig. 1, I–I'' and Fig. S1 H). Interestingly, its upstream regulators MKK7 and MKK4 were also found to be enriched at the apical surface of MCCs, but only MKK7 partially colocalized with JNK (Fig. S1 I). Overexpression of MKK7 or MKK4 led to enhanced phosphorylation of the JNK at the basal bodies, suggesting that MKK7 and MKK4 might act as upstream activators of JNK in the context of MCCs (Fig. S1 J). The above data suggested that JNK displays elevated expression and phosphorylation specifically in MCCs. To confirm this observation, we injected embryos with multicilin-GR mRNA, an inducible transcript that drives multiciliated cell differentiation. Expression of multicillin was induced at embryonic stage 11, skin was isolated from control and multicilin overexpressing embryos in stages 33–35 and used for protein extraction. Western blotting analysis confirmed that total- and pJNK protein levels are increased in multicilin-overexpressing embryos (Fig. 1 J).

We next addressed the temporal kinetics of JNK association with the basal bodies. Imaging basal bodies (RFP-Centrin) during ciliated cell intercalation revealed that JNK becomes associated with newly formed basal bodies when these are deep in the cytosol of differentiating MCCs, suggesting a possible role in ciliogenesis (Fig. 1 K). Finally, we explored the association of JNK with the basal bodies using fluorescence recovery after photobleaching (FRAP). As shown in Fig. S1 K, fluorescence recovery is rapid, suggesting that GFP–JNK1 association with the basal bodies is highly dynamic, which further suggests a signaling role rather than a scaffolding role at the basal bodies.

Overall, these data show that JNK displays elevated expression and activation in MCCs and is closely associated with the basal bodies of motile and primary cilia both in *Xenopus* as well as in mammals, raising the possibility that it may play a specific conserved role in ciliogenesis.

Super-resolution imaging combined with intermolecular FRET reveals that JNK is localized at the transition fibers of MCCs and interacts with TF components

Given the close association of JNK with the basal bodies and the elevated activity of BB-associated JNK, we moved to determine the precise localization of this kinase with respect to accessory

Chatzifrangkeskou et al.
JNK is involved in ciliogenesis

Journal of Cell Biology   2 of 17
https://doi.org/10.1083/jcb.202303052

Figure 1. **JNK is closely associated with the BBs of both motile and primary cilia. (A)** Immunostaining of stage 32 *Xenopus* embryos with anti-phospho-JNK (pJNK) and anti-acetylated-α-tubulin (ac Tubulin) to visualize cilia. pJNK is localized at the base of motile cilia. Scale bars, 10 µm. **(B–B'')** Higher magnification images of pJNK at the base of cilia. Scale bars, 1 µm. **(C)** GFP-JNK and RFP-Centrin mRNA were injected into the ventral marginal region of two blastomeres at the four-cell stage, and the embryos were observed at stage 32. JNK forms a ring around basal bodies Scale bars, 5 µm. **(D)** GRP ciliated cells of a stage 17 embryo expressing RFP-Centrin and GFP-JNK1, immunostained for acetylated tubulin. GFP-JNK1 is associated with the basal bodies in GRP ciliated cells. Scale bar, 5 µm. **(E)** Neural tube cross section of a stage 22 embryo coexpressing GFP-JNK1 and centrin2 RFP and immunostained for acetylated tubulin. Scale bar, 5 µm. **(E')** The right panels represent magnified insets marked by white squares. Scale bar, 2 µm. **(F)** Confocal immunofluorescence images of serum-starved HeLa cells showing that pJNK is localized at the base of primary cilia. Scale bar, 2 µm. **(G)** Immunofluorescent images of human nasal MCCs showing anti-acetylated tubulin and anti-pJNK showing that pJNK is localized at the base of motile cilia. Scale bar, 2 µm. **(H)** Immunofluorescent images of human nasal MCCs showing anti-acetylated tubulin and anti-tJNK. Scale bar, 2 µm. **(I–I'')** Representative confocal images of endogenous localization of acetylated tubulin and JNK (tJNK) in mouse tracheal MCCs showing apical enrichment of JNK. Scale bar, 5 µm. **(J)** Western blot analysis showing elevated pJNK and JNK protein levels in

Chatzifrangkeskou et al.
JNK is involved in ciliogenesis

Journal of Cell Biology   3 of 17
https://doi.org/10.1083/jcb.202303052

skin lysates from embryos overexpressing multicilin and controls. Quantification shows the normalized ratio of pJNK/GAPDH intensity. Data represent mean ± SEM from three independent experiments. ***, P < 0.001, unpaired two-tailed t test. **(K)** Optical section of an intercalating multiciliated cell expressing GFP-JNK1 and RFP-Centrin and stained for actin. GFP-JNK1 is associated with the basal bodies during the early stages of ciliogenesis. Scale bar, 20 μm. Source data are available for this figure: SourceData F1.

structures. Lateral views of an MCC expressing RFP-Centrin and stained for pJNK show that it localizes distally from the basal bodies and proximally to the axonemes in a ring-shaped pattern, a distribution characteristic of the TZ and TFs (Fig. 2 A). To determine the precise localization of JNK, we sought to determine its position relative to TZ and TF known protein markers using airyscan super-resolution microscopy. While the transition zone of the motile cilia in the *Xenopus* MCCs is largely unexplored, proteomic approaches of primary cilia identified three major multiprotein complexes: the MKS, NPHP, and CEP290 modules (Chih et al., 2011; Garcia-Gonzalo et al., 2011; Sang et al., 2011; Awata et al., 2014; Schouteden et al., 2015; Tony Yang et al., 2015). Thus, we initially examined the localization of selected components of these complexes in *Xenopus* epidermal MCCs using airyscan super-resolution microscopy, including CEP290, B9D1, NPHP1, TMEM216, and MKS1 (Fig. S2 A). We assessed whether the candidate proteins localized at the TZ in living embryos, like their counterparts in other organisms, express a combination of different fluorescent markers. In agreement with the TZ map from other model organisms, B9D1 is localized along the BBs, CEP290 localizes to the TZ proximal end, and NPHP1 is distal to it. Despite the similarities in protein organization within the TZ of primary and motile cilia, there are some differences between them. For instance, MKS1 and CEP290 are localized at the same lateral level (Fig. S2 A). Altogether, these results indicate that all five proteins are localized at the TZ of *Xenopus* MCCs, in agreement with reports in other organisms (Gonçalves and Pelletier, 2017).

TFs and the TZ are in very close proximity. We further focused on determining the precise localization of the best-characterized TF-associated proteins (Fig. S2 B). CEP164, a component of the TFs known to mediate the anchorage of basal bodies to the plasma membrane, was examined to establish the proximal end of the TZ. CEP164 was distributed around basal bodies and colocalized with three other TF components, CEP83, CEP123, and IFT52. Chibby clusters as rings smaller than CEP164 rings at the ciliary base (Fig. S2 B). These data confirm that the TZ and TF markers selected display a similar localization in *Xenopus* as what was previously reported in mammalian cells.

Using this super-resolution map as a reference, we next examined the precise localization of JNK. JNK was detected at the same axial level as CEP290 and MKS1 but occupied a wider area (Fig. S2 C). Interestingly, in top views, JNK was found in a ring-shaped-distribution coincident with CEP164, CEP123, CEP83, and IFT52 with a lateral diameter of ~500 nm, consistent with the transition fiber ring diameter (Stephan et al., 2007; Hu et al., 2010; Fig. 2, B and C). Collectively, our data place JNK within the area occupied by the transition fibers (Fig. 2 D). To confirm this localization and explore the possibility that JNK interacts with TF components, we carried out intermolecular fluorescence resonance energy transfer (FRET) experiments. As shown, FRET is taking place between JNK and CEP123 but not between JNK and Chibby, in agreement with our localization data (Fig. 2 E and Fig. S2 D).

Moreover, we examined the interaction of JNK with another TF core component, CEP164, by immunoprecipitation. Embryos were injected with GFP-JNK and the multicilin-GR mRNA to induce ectopic MCC differentiation. Skin from induced and control embryos was mechanically isolated, subjected to immunoprecipitation using GFP-trap beads, and analyzed by Western blotting with an antibody against CEP164 (Fig. S2 E). Overall, these data show that JNK is localized at the transition fiber region and interacts with TF components CEP123 and CEP164.

JNK activity is necessary for ciliogenesis

The above data clearly show that active JNK is associated with the basal bodies from the early stages of MCC development, suggesting a possible role in this process. To address this, we knocked down JNK using a morpholino oligonucleotide (MO) against *Xenopus* JNK (hereafter referred to as JNK MO), the specificity of which has been previously demonstrated (Yamanaka et al., 2002; Liao et al., 2006). To test the efficiency of the JNK MO KD, two cell-stage embryos were injected with morpholino (40 ng/embryo), and as shown, immunoblotting analysis showed a significant reduction of endogenous protein levels (Fig. S3 A). The *Xenopus* epidermal mucociliary epithelium generates robust fluid flow over the tadpole, thus preventing colonization and infection of the embryo by bacteria (Hayes et al., 2007; Werner and Mitchell, 2012; Nommick et al., 2022). We thus sought to investigate the role of JNK in ciliary function by initially examining the impact of JNK KD on cilia-driven fluid flow generation. To address this, we added fluorescent beads to the culture media followed by high-speed recordings of bead movement. Embryos injected with JNK MO displayed a striking reduction in flow generation compared with controls suggesting defective ciliogenesis (Fig. 3 A).

To further examine whether JNK is involved in ciliogenesis, JNK MO was injected into the ventral blastomeres of four-cell embryos. These, together with controls, were allowed to develop to stage 31/32, fixed, and stained for acetylated tubulin and centrin. Unlike control embryos, the acetylated tubulin signal intensity was drastically reduced in JNK morphants with an increased number of partially ciliated and non-ciliated cells, and a large number of basal bodies were trapped inside the cytoplasm (Fig. 3 B). At higher MO amounts (80 ng), basal bodies were almost exclusively found deep within the cell body failing to migrate to the apical surface (Fig. S3 B). By measuring the apical cell surface area, we discovered that MCCs are smaller in JNK morphants suggesting that apical expansion is also affected (Fig. 3 B). Rescue experiments using a construct that expresses mScarlet-JNK partially restored the phenotypes elicited by the
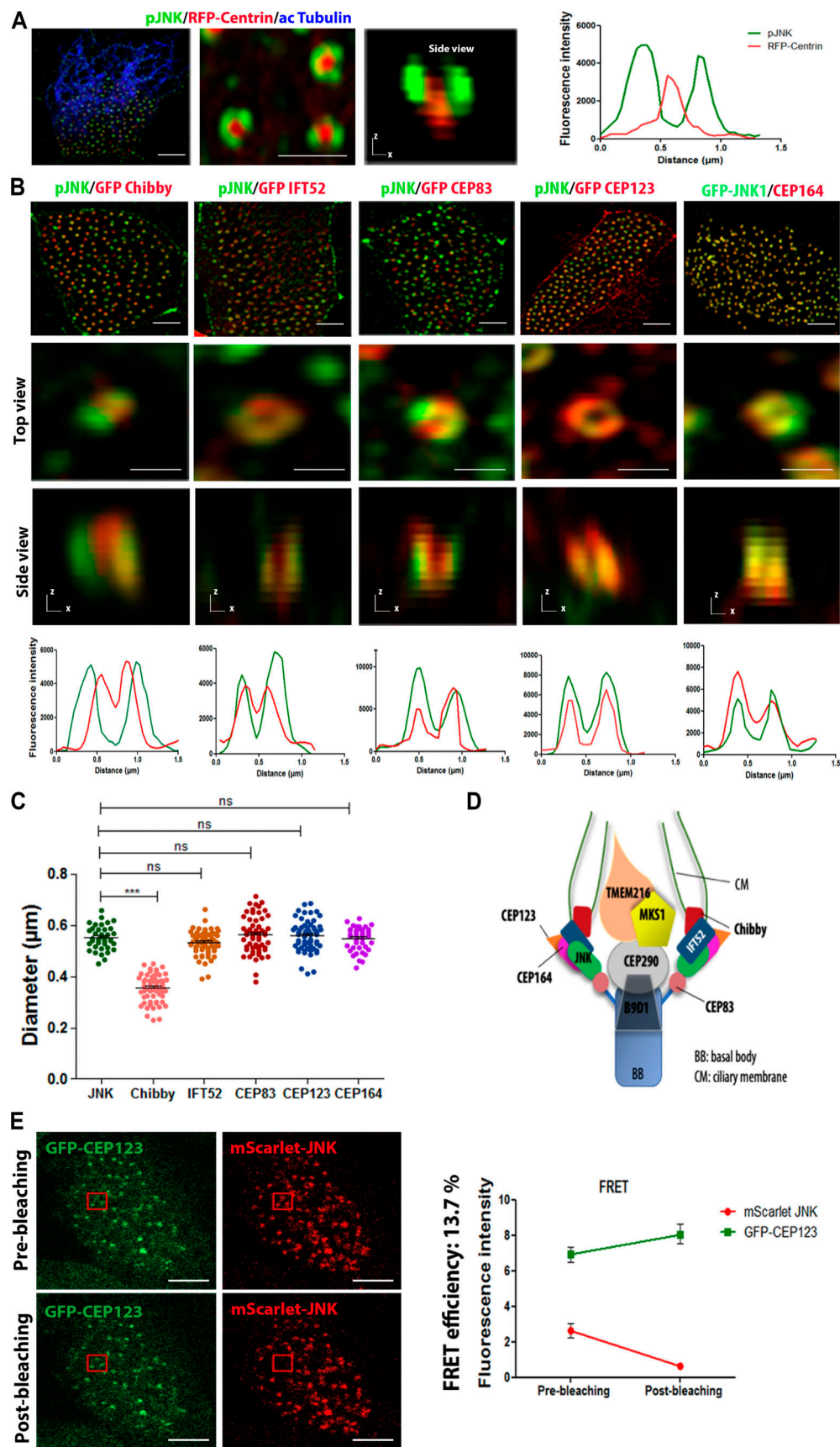
Figure 2. **Super-resolution imaging combined with intermolecular FRET reveals that JNK is localized at the transition fibers of MCCs and interacts with TF components. (A)** A *Xenopus* epidermal MCC expressing RFP-Centrin stained for pJNK and acetylated tubulin. Scale bars, 5 μm. Top-down higher

Chatzifrangkeskou et al.
JNK is involved in ciliogenesis

Journal of Cell Biology   5 of 17
https://doi.org/10.1083/jcb.202303052

magnification view is shown. Scale bars, 1 µm. Side view (XZ projection) showing that pJNK is localized distally from the basal bodies. Fluorescence intensity profile along the white arrow. **(B)** (I) Representative Z-stack images of embryos injected with GFP-Chibby and stained for pJNK. (II) Images of embryos injected with GFP-IFT52 and stained for pJNK. (III) Images of embryos injected with GFP-CEP83 and stained for pJNK. (IV) Images of embryos injected with GFP-CEP123 and stained for pJNK. (V and III) Images of embryos injected with GFP-JNK and stained for CEP164. Scale bars, 5 µm. High-magnification top views and fluorescence intensity profiles are shown. Scale bars, 0.5 µm. Side views show XZ projection. **(C)** Quantification of the mean diameters of the rings of JNK (n = 39 BBs), Chibby (n = 63 BBs), IFT52 (n = 63 BBs from 4 MCCs), CEP83 (n = 57 BBs from 3 MCCs), CEP123 (n = 60 BBs from 4 MCCs), and CEP164 (n = 40 BBs from 3 MCCs) show that JNK's ring has approximately the same diameter as IFT52, CEP83, CEP123, and CEP164. Bars represent mean ± SEM from two experiments. ***, $P < 0.001$, unpaired two-tailed t test. **(D)** Schematic diagram depicting JNK localization in relation to other markers. TZ, transition zone; BB, basal body; TF, transition fiber. **(E)** Multiciliated cell expressing mScarlet JNK (acceptor) and GFP-CEP123 (donor), before and after acceptor photobleaching. GFP intensity rises, showing that FRET is taking place between GFP and mScarlet and suggesting that JNK is interacting with CEP123. Data represent mean ± SEM (n = 5 MCCs from three embryos).

loss of JNK, confirming the specificity of the knockdown (Fig. 3 B). Given previous reports on JNK in apical/basal polarity and planar cell polarity (PCP) in zebrafish (Gao et al., 2017), we used the apical marker ZO-1 and the core PCP protein GFP-Dishevelled previously shown to localize near the base of cilia (Park et al., 2008). We observed that the localization of both markers remained unaffected upon depletion of JNK (Fig. S3, C and D). To rule out that defects in ciliogenesis might arise from secondary problems in non-MCCs, we used a dominant-negative inhibitor containing the JNK binding domain (JBD) of JNK-interacting protein-1 (JIP-1; Bonny et al., 2001; Harding et al., 2001; Barr et al., 2002; Heo et al., 2004; Stebbins et al., 2008) under the multiciliated cell-specific α-tubulin promoter. Expression of this construct led to an increased number of partially ciliated and non-ciliated cells and an increased number of MCCs with defective BB migration, showing that JNK has a cell-autonomous role in MCCs (Fig. 3 C).

We next sought to examine whether JNK kinase activity is required for ciliogenesis. To do so, we took advantage of the well-characterized selective ATP competitive JNK inhibitor SP600125. SP600125 was added to the media of stage 14 embryos before ciliogenesis begins. The efficiency of the inhibitor was confirmed by Western blot analysis (Fig. S3 E). We observed decreased fluid flow in SP600125-treated embryos, suggesting that JNK's enzymatic activity is important for ciliogenesis (Fig. 3 D). We thus went on to examine the impact of JNK inhibition on ciliogenesis. Similarly, to JNK depletion, inhibition of JNK led to impaired ciliogenesis. Inhibitor-treated tadpoles displayed defective BB migration with the majority of cells forming few or no cilia (Fig. 3 E). Similar results were obtained using the substrate–competitive inhibitor, BI-78D3 (Fig. S3, F and G). These results show that inhibition of JNK elicits a phenotype that is nearly identical to that of JNK knockdown, suggesting that JNK's role in ciliogenesis is kinase activity dependent. Given the association of JNK1 with primary cilia, we further sought to investigate whether JNK inhibition also affects primary ciliogenesis. As shown, inhibition of JNK activity in HeLa cells resulted in a significant reduction of cells forming cilia without impact on ciliary length (Fig. S3 H).

In an effort to identify potential downstream JNK candidates in MCCs, we focused on JUN, a transcription factor of the activator protein-1 (AP-1) complex and one of the most extensively studied substrates of JNK. We injected embryos with either multicilin-GR mRNA only or together with JNK MO, and the skin was isolated. Western blotting analysis showed that phospho-JUN levels are increased in multicilin overexpressing embryos and drastically decreased in multicilin/JNK MO coinjected embryos, suggesting that JUN phosphorylation is a potential downstream candidate of JNK in MCCs (Fig. 3 F).

Overall, these data show that JNK plays a critical role in both primary and motile ciliogenesis and that the role of JNK in ciliogenesis is at least partially dependent on its kinase activity.

Loss of JNK impacts the IFT-B complex and destabilizes the actin network of multiciliated cells

The above data clearly show that JNK plays a critical role during ciliogenesis. Given the association of JNK with the TF and the critical role of TF components such as CEP164 and CEP83 in ciliogenesis (Graser et al., 2007; Schmidt et al., 2012; Tanos et al., 2013), we first examined the impact of the loss of JNK on TF proteins. Depletion of JNK had no significant impact on the localization of the core proteins CEP83, CEP123, and CEP164 (Fig. S4 A); however, the association of IFT52 with the basal bodies of MCCs was dramatically reduced, suggesting that JNK may be important for its recruitment to basal bodies (Fig. 4 A). Surprisingly however, the association of IFT46, which was previously reported to be recruited to the basal bodies by IFT52 in primary cilia (Lv et al., 2017), was unaffected in JNK morphants (Fig. S4 A). To rule out the possibility that loss of IFT52 is secondary to failure of basal body migration and docking, we examined its association with BBs during the early stages of ciliogenesis. As shown, in control embryos, IFT52 becomes associated with the basal bodies at early stages (stage 19), during basal body migration, and prior to docking, suggesting that its absence in JNK morphants is not due to the failure of basal bodies to dock (Fig. S4 B). Given the fact that mutations of IFT52 lead to primary and motile ciliogenesis defects (Zhang et al., 2016), these data suggest that defects in ciliogenesis elicited by loss of JNK at least in part stem from a role of JNK in the recruitment of IFT52 to basal bodies. However, inhibition of basal body migration cannot be attributed to IFT defects, suggesting that JNK has a more complex role.

The actin cytoskeleton plays a critical role in basal body migration, and we have previously shown that disruption of basal body–actin interactions leads to similar defects (Vladar and Axelrod, 2008; Antoniades et al., 2014; Sedzinski et al., 2016; 2017). Given prior studies indicating that JNK can regulate the actin cytoskeleton (Homsy et al., 2006; Naydenov et al., 2009; Mengistu et al., 2011; Björkblom et al., 2012), we examined the impact of JNK on the actin cytoskeleton of MCCs. Intriguingly,
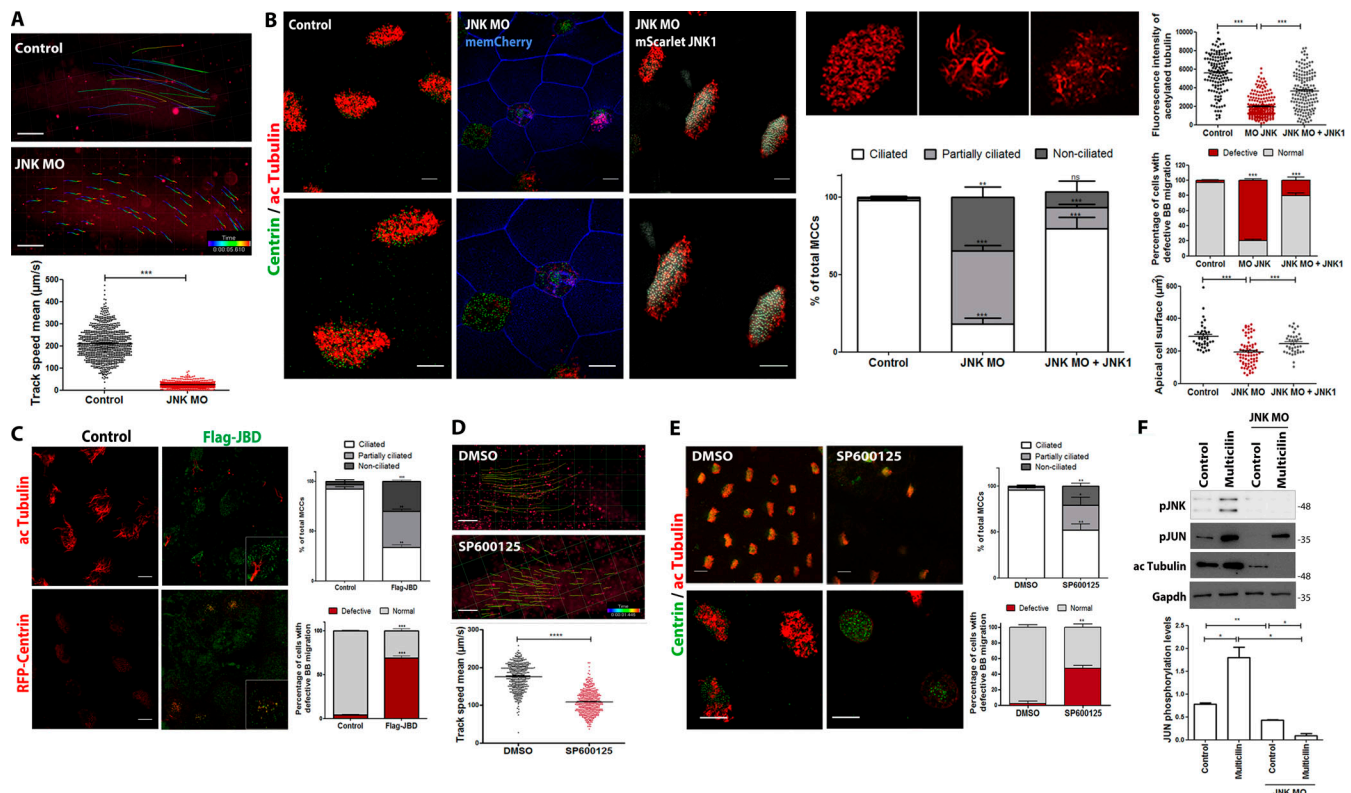
Figure 3. **JNK activity is necessary for ciliogenesis. (A)** Velocity of fluorescent beads in micrometers per second of control *Xenopus* embryos and embryos injected with JNK MO. MO (40 ng per cell) was injected into the ventral blastomeres at the four-cell stage. Scale bar, 500 μm. Quantification of the bead velocity shows impaired fluid flow in JNK morphants. Error bars indicate ± SEM from two experiments, *n* = 5 embryos (stage 29–30) per group. ***, P < 0.001, unpaired two-tailed *t* test. **(B)** Control embryos or JNK MO-injected embryos were fixed at stage 31/32 and stained for ac-tubulin and centrin. Coinjection of JNK MO with mScarlet-JNK1 rescued the ciliary defects. Scale bar, 10 μm. Quantifications of the acetylated tubulin intensity, percentage of ciliated, partially ciliated and non-ciliated cells (*n* = 305 control cells from three embryos, *n* = 398 JNK MO MCCs from four embryos, *n* = 431 from three embryos), and the percentage of cells displaying trapped basal bodies within the cytoplasm in controls (*n* = 203 MCCs from three embryos), JNK morphants (*n* = 580 from two embryos), and JNK MO/mScarlet JNK (*n* = 154 from three embryos) injected embryos. Apical cell surface area of epidermal MCCs is decreased in JNK MO-injected embryos. Error bars indicate ± SEM. **, P < 0.01, ***, P < 0.001, unpaired two-tailed *t* test. **(C)** Representative images of stage 30 control embryos or embryos injected with Flag-JBD under α-tubulin promoter. Embryos were either stained for acetylated tubulin or coinjected with RFP-Centrin to mark basal bodies. The graph shows a higher percentage of partially ciliated and non-ciliated cells (*n* = 288 MCCs from three embryos) as well as MCCs with defective BB migration in embryos injected with Flag-JBD compared with controls (*n* = 309 MCCs from three embryos). Error bars indicate ± SEM from three experiments. **, P < 0.01, ***, P < 0.001, unpaired two-tailed *t* test. Scale bar, 10 μm. **(D)** Quantification of the fluid flow with fluorescent beads shows decreased bead velocity in SP600125-treated embryos compared to DMSO. Error bars indicate ± SEM, *n* = 5 embryos (stage 29–30) per group. ****, P < 0.0001, unpaired two-tailed *t* test. Scale bar, 500 μm. **(E)** Confocal imaging of cilia in DMSO- and SP600125-treated stained with anti-acetylated tubulin and of basal bodies stained with anti-Centrin. Scale bars, 20 μm. Graph showing a higher percentage of partially ciliated and non-ciliated MCCs (*n* = 272 control cells from 5 embryos, *n* = 259 SP600125-treated cells from 6 embryos) and cells displaying defective basal body migration in SP600125-treated embryos (*n* = 118 from 5 embryos) compared with control (*n* = 120 from 5 embryos). Error bars indicate ± SEM from three experiments. *, P < 0.05, **, P < 0.01, unpaired two-tailed *t* test. **(F)** Western blot showing phospho-JUN levels in skin lysates from uninjected, multicilin overexpressing, and multicilin/JNK MO coinjected embryos. Quantification shows the normalized ratio of pJUN/GAPDH intensity. Data represent mean ± SEM from two independent experiments. *, P < 0.05, **, P < 0.01, unpaired two-tailed *t* test. Source data are available for this figure: SourceData F3.

JNK knockdown led to a significant reduction of fibrillar actin in MCCs, disorganization of the apical actin network, and near elimination of the subapical network (Fig. 4 B). The apical network was dramatically affected with actin forming discontinous filaments rather than the typical highly organized interwoven network seen in controls. Likewise, inhibition of JNK activity also led to impaired apical and subapical actin networks, suggesting that JNK kinase activity is required for the establishment of the complex MCC actin networks (Fig. S4 C).

The organization defects observed in JNK morphants shown by the weak and discontinuous actin staining suggested that loss of JNK led to the destabilization of the robust fibrillar actin network in these cells. To address this possibility directly, we carried out FRAP experiments in control and morphant embryos expressing mKate2 actin (Fig. 4 C). A small region of the apical actin network was photobleached, and the recovery was then monitored. The recovery of apical actin in ciliated cells of JNK morphants was significantly faster (t1/2 = 28.3 s; Fig. S4 D) than in controls (t1/2 = 83 s; Fig. S4 D), and the immobile fraction within the time frame of the experiment drastically reduced from 21.6 to 5.8% (Fig. 4 C), suggesting that the apical actin network is far more dynamic in morphants than controls. These data confirm that in the absence of JNK, ciliated cells are unable to stabilize the apical actin network.
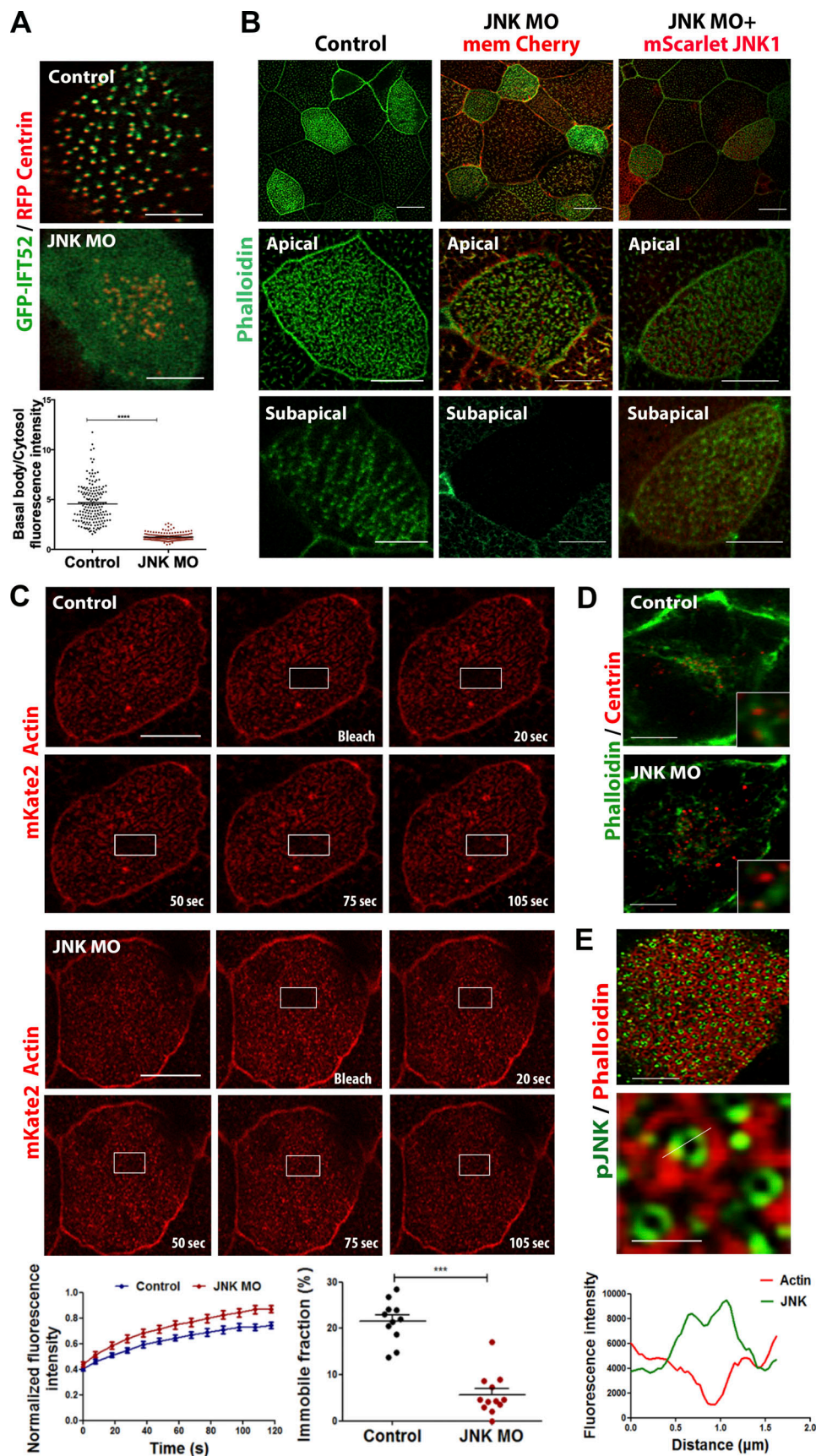
Chatzifrangkeskou et al.
JNK is involved in ciliogenesis

Journal of Cell Biology 7 of 17
https://doi.org/10.1083/jcb.202303052

Figure 4. **Loss of JNK impacts the IFT-B complex and destabilizes the actin network of multiciliated cells. (A)** Representative images from control and JNK morphant embryos injected with RFP-Centrin and GFP-IFT52. Scale bars, 10 µm. Quantification of the fluorescence intensity ratio of GFP-IFT52 shows

Chatzifrangkeskou et al.
JNK is involved in ciliogenesis

Journal of Cell Biology   8 of 17
https://doi.org/10.1083/jcb.202303052

impaired recruitment of IFT52 on basal bodies in JNK MO MCCs. Data represent mean ± SEM from three independent experiments. ****, P < 0.0001, unpaired two-tailed *t* test. **(B)** Immunofluorescence showing *Xenopus* epidermal MCCs labeled for F-actin (Phalloidin) in controls, embryos injected with JNK MO, or JNK MO/mScarlet JNK. Membrane-mCherry mRNA was used as a lineage tracer. Single optical sections at the level of apical and subapical actin layers show defective networks in JNK morphants. Scale bars, 10 μm. **(C)** Fluorescence recovery after photobleaching (FRAP) experiment on a stage 33 embryo with docked basal bodies, expressing either mKate2-actin alone or mKate2-actin with JNK MO. Normalized graph of FRAP experiment depicting signal intensity of bleached region over time shows faster recovery of apical actin and decreased immobile fraction in JNK MO (n = 8 MCCs from four embryos) MCCs compared with controls (n = 6 MCCs from three embryos). Error bars indicate ± SEM from two experiments. ***, P < 0.001, unpaired two-tailed *t* test. Scale bars, 10 μm. **(D)** Intercalating ciliated cells of stage 17 from control or JNK MO-injected embryos were stained for Phalloidin and centrin to label actin network and basal bodies, respectively. MCCs of JNK morphants show a defective association of basal bodies with the actin network. **(E)** Immunofluorescence image showing MCCs labeled for F-actin (Phalloidin) and pJNK. Scale bars, 10 μm. High-magnification top view and fluorescence intensity profile along the white line show that pJNK is interwoven within the apical actin network. Scale bars, 2 μm.

Actin and myosin are both essential for the migration of nascent basal bodies to the apical surface (Lemullois et al., 1988; Boisvieux-Ulrich et al., 1990; Antoniades et al., 2014; Walentek et al., 2016; Tu et al., 2018). Given the basal body migration defects observed in JNK morphants and the defects of the actin networks in mature MCCs, we went on to examine the possibility that actin–BB interactions are disrupted earlier, during BB migration (Fig. 4 D). As shown in controls, basal bodies are surrounded by a complex actin network while morphant cells display a disorganized network with basal bodies failing to properly associate with actin. This suggests that the defects in BB migration elicited by JNK downregulation and pharmacological inhibition are rooted in the role of JNK in the regulation of actin.

Given the critical role of JNK in the regulation of the complex actin networks of MCCs, we then asked if JNK associates with actin in these cells, similar to that previously reported in adherent cells (Christerson et al., 1999; Yang et al., 2007). Super-resolution imaging of phospho-JNK and actin reveals that active JNK is interwoven within the apical actin network frequently displaying partial colocalization (Fig. 4 E). In addition, we occasionally detected a second region of JNK enrichment forming below the basal bodies, in close association with the subapical actin (Fig. S4 E). To confirm the close spatial relationship and examine a possible interaction between JNK and the actin network, we carried out intermolecular FRET experiments. We coexpressed GFP-JNK (donor) with mKate2 actin (acceptor) and carried out acceptor photobleaching. As shown, FRET is taking place between GFP and mKate2 in MCCs, confirming the proximity of JNK with actin and suggesting a possible interaction (Fig. S4 F), consistent with a previously shown interaction of JNK with α actinin and in line with the role of JNK in the regulation of actin networks in multiciliated cells (Yang et al., 2007). Overall, these data suggest that JNK's involvement in ciliogenesis stem from its role in the recruitment of IFT52, a critical IFT-B complex member and in the regulation of the complex actin networks driving multiple aspects of MCC development.

JNK activity is necessary for ciliary function
The association of JNK with the basal bodies of both differentiating as well as fully differentiated cells suggests roles in both the development as well as the function of MCCs. To address a possible role of JNK in ciliary function, we treated embryos with the selective JNK ATP competitive inhibitor, SP600125, after

MCCs differentiation was completed (stage 31–34). Immunoblotting analysis of extracts from tadpoles' skin showed that levels of pJNK are significantly reduced following a 2-h treatment (Fig. S5 A). We first evaluated ciliary function by monitoring the flow of fluorescently labeled beads over the tadpoles' skin and by measuring ciliary beating frequency (CBF) after a 2-h treatment. Both CBF and the rate of displacement of individual beads were significantly reduced in embryos treated with the JNK inhibitor (Fig. 5 A and Fig. S5 B). This suggests that JNK kinase activity is essential for MCC function.

We went on to explore the mechanism through which JNK inhibition suppresses MCC flow generation. We performed immunostaining using an antibody against acetylated tubulin. The intensity of acetylated tubulin in SP600125- or BI-78D3-treated embryos was not significantly different from DMSO-treated embryos, suggesting that JNK inhibition did not elicit loss of cilia (Fig. 5 B and Fig. S5 C). Staining with phalloidin showed that the apical cell surface in treated embryos was reduced (Fig. 5 B and Fig. S5 C). Given the disruption of the actin networks in JNK morphants, we went on to examine the actin cytoskeleton in inhibitor-treated embryos. Remarkably, the apical actin meshwork that surrounds each basal body as well as the subapical actin network were largely disrupted in 2-h SP600125- and BI-78D3-treated embryos, suggesting that JNK activity is required for the maintenance of the apical and subapical actin networks in MCCs (Fig. 5 C and Fig. S5 D). The effect of JNK on actin is reversible upon drug washout (Fig. S5 E). To examine whether the reduction of the apical cell surface elicited defects in the basal body spacing, we quantified the distance between individual basal bodies and their nearest neighbors. As shown in JNK inhibition, the distance between basal bodies is drastically decreased (Fig. 5 D) without affecting rotational polarity (Fig. S5 F). The reduced distance between basal bodies is due to a reduction of the apical surface since the number of basal bodies remains unchanged upon JNK inhibition (Fig. S5 G).

Of note, 2-h JNK inhibition did not affect IFT-52 association with the basal bodies (Fig. S5 H). Collectively, these data reveal a critical role of JNK in the regulation of the apical and subapical actin networks of MCCs and consequently in MCC-driven fluid flow generation.

Discussion
Cilia can produce mechanical force for locomotion or fluid flow or sense extracellular signals that modulate developmental
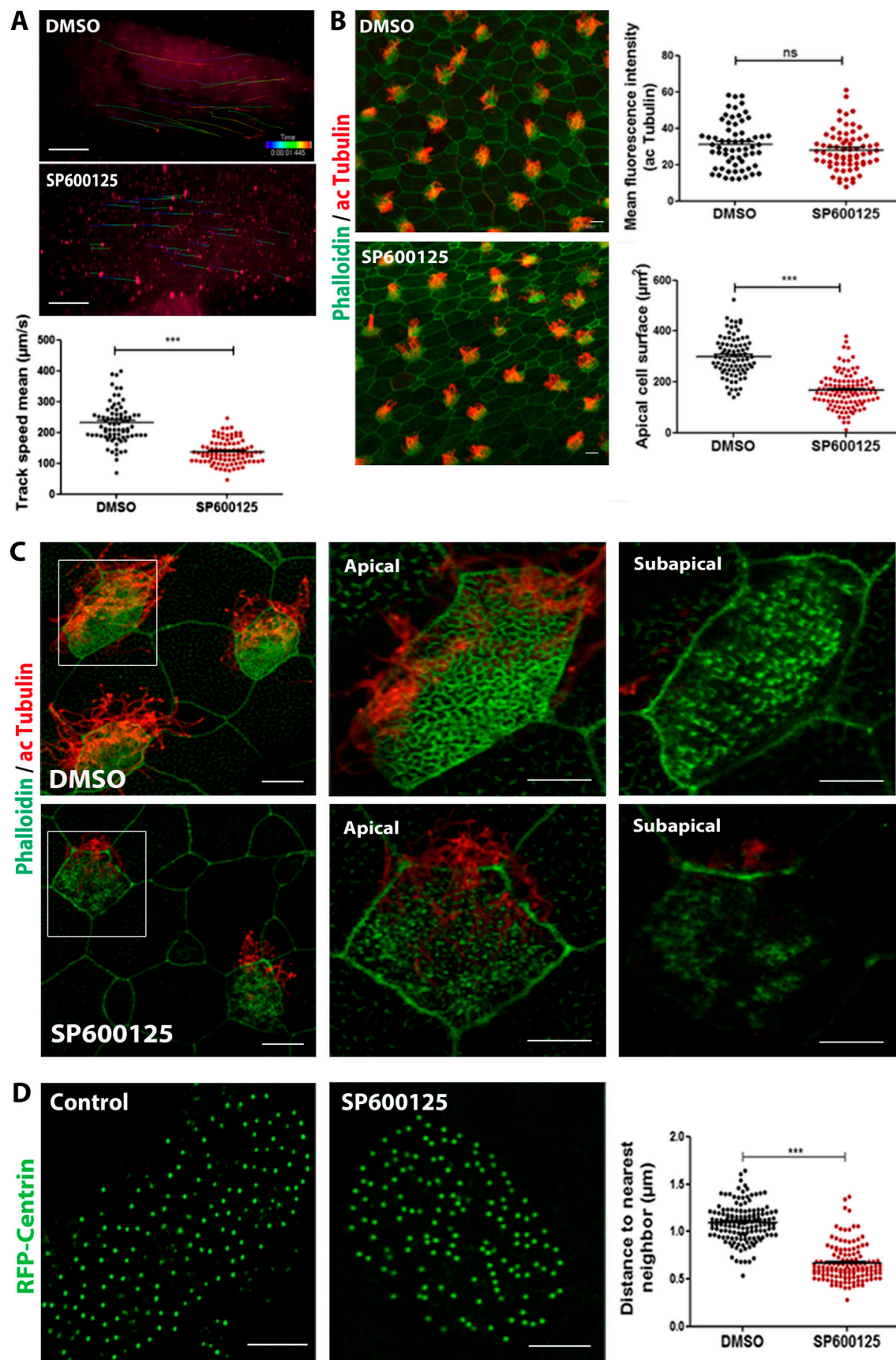
Figure 5.   **JNK activity is necessary for ciliary function. (A)** Quantification of the fluid flow with fluorescent beads in DMSO- and SP600125-treated (2 h) embryos. SP600125 was added into the media of embryos after MCC differentiation was completed, at stages 31–34. Error bars indicate ± SEM from two

independent experiments, *n* = 5 embryos per group, ***, P < 0.001, unpaired two-tailed *t* test. Scale bar, 500 μm. **(B)** Immunofluorescence images showing *Xenopus* epidermal MCCs labeled for F-actin (Phalloidin) and cilia (anti-acetylated α-tubulin) after exposure to DMSO or SP600125 for 2 h. Scale bars, 20 μm. Quantification shows decreased acetylated tubulin intensity (*n* = 63 DMSO, *n* = 70 SP600125) and apical cell surface in SP600125-treated embryos (*n* = 107 MCCs) compared with DMSO (*n* = 87). Error bars indicate ± SEM from three experiments. ***, P < 0.001, unpaired two-tailed *t* test. **(C)** Higher magnification images of 2 h DMSO- and SP600125-treated MCCs stained for Phalloidin and acetylated α-tubulin. The apical and subapical actin networks in SP600125-treated embryo are impaired. Scale bars, 10 μm. **(D)** RFP-Centrin injected embryos were treated for 2 h at stage 30 with either DMSO- or SP600125. Quantification of basal body distribution by measuring the distance of individual basal bodies relative to their nearest neighbors (*n* = 140 basal bodies for each condition from three embryos). Error bars indicate ± SEM from three experiments. ***, P < 0.001, unpaired two-tailed *t* test.

---

pathways, ultimately regulating cell proliferation and differentiation (Drummond, 2012). Both motile and primary cilia are assembled by an intraflagellar transport (IFT) machinery, a microtubule motor-based movement of ciliary proteins along the axoneme (Pedersen et al., 2008). Cilia harbor a "ciliary gate" that can be divided into two structurally distinct regions: the transition fibers and the transition zone. Several studies have led to the discovery of a growing number of TZ and TF proteins and protein complexes, many of which are associated with ciliopathies (Hu et al., 2010; Garcia-Gonzalo et al., 2011; Sang et al., 2011; Williams et al., 2011; Reiter et al., 2012). Here, we analyzed the localization of various TZ and TF proteins in *Xenopus* MCCs using airyscan microscopy. The localization patterns and protein distribution are in broad agreement with earlier studies in mammals showing that the TZ in *Xenopus* MCCs is conserved both in terms of composition and architecture. Together with the transition fibers, the TZ forms a selective gate that is responsible for the protein and lipid composition of cilia. Despite critical roles in ciliary function as well as its involvement in human disease, how this gate is established and fulfills its functions remains unclear, and both the TZ and TF remain poorly characterized both in terms of composition as well as regulation (Gonçalves and Pelletier, 2017). We now show that JNK is a novel component and regulator of these structures. JNK is localized at the transition fiber region of cilia together with IFT52, CEP164, CEP123, and CEP83. While JNK has well-established roles in stress responses and apoptosis, our results uncover a novel role in MCC development and function.

Recent work shows that JNK acts at different points during left–right axis establishment in zebrafish, distinct from the PCP signaling pathway (Derrick et al., 2022) and regulates nodal cilia length (Gao et al., 2017). Here, we show that loss of JNK in *Xenopus* MCCs led to serious defects in ciliogenesis, including defective migration and docking of the basal bodies and fewer cilia projecting above the surface of the MCCs. Importantly, JNK appears to be critical for both MCC development but also for primary ciliogenesis. The function of JNK in both primary and motile ciliogenesis is at least in part dependent on its kinase activity. Despite the fact that the underlying mechanism is not entirely clear, our work demonstrates that JNK is a critical regulator of the complex actin networks of MCCs and in addition appears to control the composition of the TF. Several lines of evidence support the critical role of the actin cytoskeleton in basal body migration and docking (Park et al., 2008; Ioannou et al., 2013; Antoniades et al., 2014; Brooks and Wallingford, 2014; Epting et al., 2015). The phenotypes observed upon JNK knockdown or inhibition are suggestive of defects in the regulation of the actin cytoskeleton. JNK becomes associated with the

basal bodies before they dock to the apical surface and is critical for the stabilization of both the apical and subapical actin networks in MCCs. Not surprisingly, several actin modulators have been found to associate with the basal bodies, and it is clear that both apical and subapical actin networks established at MCCs are controlled and regulated by proteins residing at the basal body (Huang et al., 2003; Park et al., 2008; Antoniades et al., 2014; Chevalier et al., 2015; Epting et al., 2015; Kulkarni et al., 2018; Yasunaga et al., 2022). Thus, JNK is joining other actin regulators shown to associate with the basal bodies and coordinate the establishment and maintenance of the complex actin networks critical for MCC differentiation and function.

The role of JNK is not restricted to the establishment of these networks but is also required for their maintenance. Our data reveal that JNK inhibition in fully differentiated MCCs leads to actin network destabilization and basal body spacing defects, which as a consequence lead to the reduction of MCC-generated flow and defects in mucociliary clearance. These data are consistent with the constitutive association of pJNK with the basal bodies and suggest that continuous JNK signaling is required to sustain the complex actin networks of MCCs.

JNK has a clear role in the regulation of the actin network and this role clearly underlies some of the defects observed in morphants such as basal body migration and docking defects; however, its role in MCC development goes beyond actin regulation. Our data suggest that defects in ciliogenesis elicited by loss of JNK may at least in part stem from a role of JNK in the recruitment of IFT52, a key component of the IFT-B complex, to the basal body. This is in agreement with studies suggesting that transition fiber components are important docking and assembly sites for IFT proteins (Graser et al., 2007; Sillibourne et al., 2011; Schmidt et al., 2012; Joo et al., 2013; Tanos et al., 2013; Tateishi et al., 2013; Burke et al., 2014; Ye et al., 2014). For instance, in the absence of CEP164 or CEP83, the recruitment of IFT proteins is defective (Schmidt et al., 2012; Joo et al., 2013; Tanos et al., 2013; Čajánek and Nigg, 2014). IFT-B subunits, such as IFT52 are mutated in skeletal ciliopathies (Zhang et al., 2018; Dupont et al., 2019), and loss of IFT52 was shown to impair the recruitment of several IFT-B anterograde transport complex proteins such as IFT46, IFT74, IFT81, IFT88, and ARL13B, and lead to ciliogenesis defects (Taschner et al., 2014; Zhang et al., 2016; Lv et al., 2017). The precise impact of the loss of JNK signaling on the composition and regulation of the TZ and TFs remain to be elucidated, especially with respect to primary cilia; however, changes such as loss of IFT52 would impair ciliary function both in primary as well as in motile cilia. The JNK pathway has been implicated in the pathogenesis of several diseases, including type-2 diabetes (Yung and Giacca, 2020),

obesity (Yung and Giacca, 2020) and cancer (Bubici and Papa, 2014), atherosclerosis (Wang et al., 2018), Alzheimer's disease (Solas et al., 2023), polycystic kidney disease (Smith et al., 2021), and Parkinson's (Wang et al., 2004), several of which have direct links to ciliary dysfunction. For example, primary cilia have been shown to act as protective elements that can inhibit the progress of atherosclerosis (Egorova et al., 2011; Wang et al., 2021); the central role of cilia in polycystic kidney disease is well documented (Ma, 2021) and defects in ciliary function manifest in metabolic disorders such as obesity and type 2 diabetes in human ciliopathy syndromes (Vaisse et al., 2017; Volta and Gerdes, 2017). Our findings raise the possibility that the involvement of JNK in such diseases may at least in part stem from its role in ciliogenesis and ciliary function. JNK pathway inhibitors are in development for the treatment of neurodegenerative diseases (Wang et al., 2004; Yarza et al., 2016), cancer (Wu et al., 2020), and fibrotic diseases (Grynberg et al., 2017; Popmihajlov et al., 2022), and this work suggests that the JNK pathway should also be explored as a therapeutic target through its impact on ciliary function.

Materials and methods

Embryo manipulations and microinjections
Female adult *Xenopus laevis* were ovulated by injection of human chorionic gonadotropin. Eggs were fertilized in vitro, dejellied in 1.8% cysteine (pH 7.8), and subsequently reared in 0.1× Marc's modified ringers (MMR) and staged according to Neiuwkoop and Faber. For microinjections, embryos were placed in a solution of 4% Ficoll in 0.33× MMR and injected using a glass capillary pulled needle, forceps, a Singer Instruments MK1 micromanipulator, and a Harvard Apparatus pressure injector. For most experiments, injections were made into the ventral blastomeres to target the epidermis at the four-cell or eight-cell stage. Embryos were allowed to develop to the appropriate stage and then imaged live or fixed in MEMFA for 1–2 h at room temperature (RT). For live imaging, embryos were anesthetized in 0.01% benzocaine in 0.1× MMR. To target cilia on GRP, constructs were injected into both marginal dorsal blastomeres of embryos at the four-cell stage, and embryos were fixed in MEMFA and manually dissected at stage 17.

X. laevis adults are maintained in agreement with the EU guidelines and the guidelines of the Veterinary Services of the Ministry of Agriculture, Natural Resources and Environment of the government of Cyprus. *X. laevis* are housed in our licensed facility (license number CY.EXP.102 at the University of Cyprus).

DNA constructs and morpholino oligonucleotide
The plasmids GFP-JNK1(#86830), mCherry-CEP290 (#27380), mCherry-TMEM216 (#41633), mEmerald-MKS1 (#54183), mEmerald-B9D1 (#54011), mEmerald-NPHP1 (#54204), GFP-Chibby (#89472), GFP-CEP123 (#67787), GFP-CEP83 (#128874), GFP-IFT52 (#128875), Flag-MKK4 (#14615), and Flag-MKK7 (#14538) were obtained from Addgene. mCherry-IFT46 was a gift from Kazuhisa Nakayama (Kyoto University, Kyoto, Japan). Rescue experiments were performed by coinjection of capped

RNA encoding human JNK. Capped RNA was prepared with the SP6 mMessage mMachine Kit (Ambion) using linearized plasmids. The JNK MO used was 5′-TGCTGTCACGCTTGCTTCGGC TCAT-3′. mRNA of Centrin-RFP (80 pg), Clamp-GFP (100 pg), mem-Cherry (50 pg), and mKate-Actin/RFP-Utrophin (120 pg) were injected to mark basal bodies, ciliary rootlets, membrane, and F-actin, respectively. For α-tubulin-driven expression of Flag-JBD, the Flag-JBD was amplified by performing PCR from a plasmid obtained from Addgene (#15751), enzymatically subcloned into a α-tubulin-driven expression plasmid, and injected into two ventral blastomeres at the four-cell stage at 50 pg per blastomere.

JNK inhibitor treatment
Drug treatment with SP600125 (50 µM; Calbiochem) and BI-78D3 (20 µM; Calbiochem) was performed at stage 14 or as otherwise stated. After the drug was added to the culture medium (0.1× MMR), embryos were incubated in the presence of the drug overnight at 16°C until they reached stage 32–35. When embryos were treated at stage 31–34, they were incubated in the presence of the drug for 2 h at 16°C.

Cell culture
HeLa cells were cultured under standard conditions in DMEM culture media supplemented with 10% FBS at 37°C and 5% CO_2. For the induction of primary cilia, a serum starvation medium was used for 24 h in the presence of DMSO or 10 µM SP600125.

Air–liquid interface differentiation of primary human nasal airway cells
Human primary nasal airway cells from healthy volunteers were collected using a cytology brush by a nurse, with a protocol approved by the Cyprus National Bioethics Committee (EEBK/EΠ/2013/21). All patients gave their written informed consent. Airway cells were then expanded, seeded on transwells (Corning HTS Transwell-96 and -24 permeable support; 0.4 µm pore size), and differentiated for at least 21 d following Stem Cell Technologies protocols using PneumaCult-Ex and PneumaCult-ALI media. The media were supplemented with vancomycin, tobramycin, gentamicin, and antibiotic–antimycotic antibiotics.

FRAP analysis
Tadpoles expressing mKate2-actin expressing embryos were anesthetized in 0.01% Benzocaine in MMR and immobilized in silicone grease wells on glass slides. A small area of an mKate2-actin positive MCC was imaged on Zeiss 900 and a 546-nm laser was used both during acquisition (1.5%) and bleaching (100%). A total of 20 frames were acquired at 10-s intervals. One frame was acquired as a prebleaching control and a rectangular ROI was bleached within one frame. Embryos were injected with RFP-Centrin/GFP-JNK, and a small area of GFP was subjected to FRAP using a 488-nm laser (acquisition 0.5%, bleaching 100%). A total of 30 frames were acquired at 5-s intervals.

The Zeiss Zen 3.0 software was used for FRAP analysis. The fluorescence recovery curve was fitted by a single exponential function given by:

$$F(t) = A(1 - e^{-R}) + B,$$

where $F(t)$ is the intensity as time t; A and B are the amplitudes of the time-dependent and time-independent terms, respectively; τ is the lifetime of the exponential term (time constant), and the recovery rate is given by:

$$R = \frac{1}{\tau}.$$

Acceptor photobleaching FRET
Stages 32–35 embryos expressing the JNK FRET biosensor were anesthetized in 0.01% benzocaine in MMR and immobilized in silicone grease wells on glass slides. A 458-nm laser was used for excitation (CFP excitation) and emission was recorded using the lambda mode for spectral imaging (λ scan). Spectral unmixing of the acquired images revealed one emission peak at 478 nm (maximum emission of CFP) and a second one at 527 nm (maximum emission of YFP). The YFP/CFP intensity ratio for each selected region was divided by the mean cytosolic YFP/CFP ratio to normalize any differences at the expression level of individual cells and embryos.

Embryos expressing GFP JNK and mKate2 Actin or mScarlet JNK together with GFP-CEP123 or GFP-Chibby were used for FRET analysis. A 543-nm laser was used for acceptor photobleaching (100% power) within a region of interest (ROI). A 488-nm laser was used for the acquisition of the donor, and emission was detected between 493 and 538 nm. One frame was acquired as a prebleaching control and the ROI (rectangular region) was bleached within one frame. Zeiss Zen 3.0 software was used for FRET analysis. FRET efficiency was calculated using the following equation:

$$FRET\ efficiency = \frac{Donor\ Post - Donor\ Pre}{Donor\ Post} \times 100$$

(Donor Post: donor emission intensity after photobleaching; Donor Pre: donor emission intensity before photobleaching).

Fluid flow assay
For the assessment of fluid flow, 31/32-stage embryos were anesthetized in 0.01% benzocaine in 0.1× MMR and FluoSpheres (F8816; Invitrogen) were added to the media. We carried out time-lapse microscopy using the Zeiss Axio Imager Z1 using a Zeiss Axiocam MR3, the Axiovision software 4.7. The frame rate of acquired movies was 20 s/2 frames per s. Tracking and quantification of flow velocities was performed using the IMARIS Software.

CBF analysis
Image of cilia beating was performed on a ZEISS Axiovert 200 M microscope equipped with a Basler scA640 video camera (Basler Vision Technologies). Analysis and measurement of CBF were performed using the Sisson-Ammons Video Analysis System.

Immunostaining
Whole-mount immunostaining of *Xenopus* embryos was carried out as previously described (Chatzifrangkeskou and Skourides, 2022). Briefly, fixed embryos were permeabilized in PBDT (1× PBS + 0.5% Triton X-100 + 1% DMSO) at RT and blocked in PBDT + 1% donkey serum for 1 h at RT. Primary antibodies were added to the blocking solution and embryos were incubated overnight at 4°C. Mouse trachea was harvested from euthanized adult mice and fixed in 4% PFA overnight at 4°C. The primary antibodies used were acetylated tubulin mouse monoclonal (#23950, 1:500; Santa Cruz Biotechnology), Centrin-1 (#12794-1-AP, 1:500; Proteintech), pJNK (#4668, 1:200; Cell Signaling), tJNK (#9252; 1:100; Cell Signaling), γ-tubulin (#7396, 1:500; Santa Cruz Biotechnology), CEP164 (#22227-1-AP, 1:300; Proteintech), and ZO-1 (#21773-1-AP, 1:200; Proteintech). The next day, the embryos were washed 3 × 10 min in PBDT. Samples were then incubated in secondary antibodies (at a dilution of 1:500)—anti-mouse Alexa 488 (Invitrogen) or anti-mouse IgG-CFL 647 (Santa Cruz Biotechnology)—at RT for 1 h. Actin labeling was performed using Alexa Fluor Phalloidin 488 or 568 (1:500; Invitrogen) at RT for 1 h. Embryos were then washed 3 × 10 min in PBDT. The GRP was manually dissected from MEMFA-fixed GFP-JNK1/RFP-Centrin injected embryos at stage 17 and post-fixed for a further 15 min. GRP tissue was then used for immunofluorescence using anti-acetylated tubulin antibody.

Starved HeLa cells and human nasal cells were fixed in 4% PFA for 10 min, permeabilized with 0.5% Triton X-100 in PBS for 10 min, and then blocked with PBS containing 1% Donkey serum for 1 h at room temperature. Cells were stained with the indicated antibodies.

Image analysis and quantifications
Images were captured using a Airycan Zeiss LSM900 confocal microscope. The orthogonal projections were generated using Zen 3.2 and final figures were made in Adobe Photoshop. Quantification of fluorescence intensity and cell surface was performed using the Zen 3.2 software. Basal body spacing was calculated by measuring the distance of each basal body to its nearest neighbor using the Zen 3.2 software. The quantification of cilia orientation was scored as previously described (Mitchell et al., 2007; Park et al., 2008) by measuring the angle of orientation of the rootlets relative to the anterior–posterior axis of the embryo. Oriana 3 software was used for the graphical representation of the data and to calculate the CSD.

Immunoprecipitation, SDS-PAGE, and Western blotting
Embryos were injected with Multicilin-hGR and induced with 5 μM dexamethasone at gastrula stage 11. The skin of stages 29–32 tadpoles was mechanically isolated using hair knives and forceps and the deep cells (inner layer in contact with the basal membrane) were removed using calcium (Ca^{2+}) and magnesium (Mg^{2+}) free buffer (CMFM)-containing EDTA. The skin was collected, and protein lysates were prepared by sonicating embryos in ice-cold MK's modified lysis buffer (50 mM Tris, pH 8.0, 150 mM NaCl, 0.5% NP-40, 0.5% Triton X-100, 100 mM EGTA, and 5 mM NaF) and supplemented with protease inhibitors (1 mM phenylmethylsulfonyl fluoride and protease cocktail; Sigma-Aldrich). Homogenates were cleared by centrifugation at 15,000 × g for 15 min at 4°C. Lysates were incubated with GFP-trap beads (Chromotek) for 2 h. After washing,

2× SDS loading dye was added to the beads and denatured at 95°C for 5 min to elute captured proteins.

Proteins were separated on 10% SDS-polyacrylamide gels with the BlueStar prestained ladder (NIPPON Genetics) and blotted onto nitrocellulose membranes (Sigma-Aldrich). Blots were blocked in 5% BSA in PBST (1 × PBS buffer and 0.1% Tween 20) and then incubated with the primary antibodies overnight at 4°C. The primary antibodies used were acetylated tubulin mouse monoclonal (#23950, 1:1,000; Santa Cruz Biotechnology), GAPDH (#32233, 1:2,000; Santa Cruz Biotechnology), pJNK (#4668, 1:1,000; Cell Signaling), tJNK (#9252, 1:1,000; Cell Signaling), GFP (#AB0020-200, 1:3,000; SICGEN), CEP164 (#22227-1-AP, 1:1,000; Proteintech), and phospho-JUN (#28891-1-AP, 1:1,000; Proteintech). Visualization was performed using horseradish peroxidase-conjugated antibodies (anti-rabbit and anti-mouse, 1:5,000; Santa Cruz Biotechnology) after 1 h incubation at RT. The blots were developed using ECL Immobilon Forte substrate (Millipore) and imaged on a ChemiDoc Touch imager (Bio-Rad).

Statistics

Statistical analysis was performed with the GraphPad Prism software (Version 7.01). Statistical significance is reported in the figures and legends. Quantifications of changes in protein level were calculated using ImageJ software from NIH. Statistical analysis was performed using two-tailed unpaired t tests or otherwise stated, with 95% confidence interval.

Online supplemental material

Fig. S1 shows that pJNK and its upstream activators are associated with the basal bodies of motile cilia. Fig. S2 shows an airyscan super-resolution map of TZ and TF proteins in *Xenopus* motile cilia. Fig. S3 shows that knockdown or inhibition of JNK leads to motile and primary ciliogenesis defects. Fig. S4 shows that JNK is not essential for the correct targeting of other TF proteins but its activity is important for the establishment of apical and subapical actin networks. Fig. S5 shows that short-term inhibition of JNK leads to defects in CBF and apical actin without affecting rotational polarity.

Data availability

The datasets used and/or analyzed during the current study are available from the corresponding author upon request.

References

Antoniades, I., P. Stylianou, and P.A. Skourides. 2014. Making the connection: Ciliary adhesion complexes anchor basal bodies to the actin cytoskeleton. *Dev. Cell.* 28:70–80. https://doi.org/10.1016/j.devcel.2013.12.003

Awata, J., S. Takada, C. Standley, K.F. Lechtreck, K.D. Bellvé, G.J. Pazour, K.E. Fogarty, and G.B. Witman. 2014. NPHP4 controls ciliary trafficking of membrane proteins and large soluble proteins at the transition zone. *J. Cell Sci.* 127:4714–4727. https://doi.org/10.1242/jcs.155275

Barr, R.K., T.S. Kendrick, and M.A. Bogoyevitch. 2002. Identification of the critical features of a small peptide inhibitor of JNK activity. *J. Biol. Chem.* 277:10987–10997. https://doi.org/10.1074/jbc.M107565200

Benoit, B., A. Baillet, and C. Poüs. 2021. Cytoskeleton and associated proteins: Pleiotropic JNK substrates and regulators. *Int. J. Mol. Sci.* 22:8375. https://doi.org/10.3390/ijms22168375

Björkblom, B., A. Padzik, H. Mohammad, N. Westerlund, E. Komulainen, P. Hollos, L. Parviainen, A.C. Papageorgiou, K. Iljin, O. Kallioniemi, et al. 2012. c-Jun N-terminal kinase phosphorylation of MARCKSL1 determines actin stability and migration in neurons and in cancer cells. *Mol. Cell. Biol.* 32:3513–3526. https://doi.org/10.1128/MCB.00713-12

Boisvieux-Ulrich, E., M.C. Lainé, and D. Sandoz. 1990. Cytochalasin D inhibits basal body migration and ciliary elongation in quail oviduct epithelium, *Cell Tissue Res.* 259:443–454. https://doi.org/10.1007/BF01740770

Bonny, C., A. Oberson, S. Negri, C. Sauser, and D.F. Schorderet. 2001. Cell-permeable peptide inhibitors of JNK: Novel blockers of β-cell death. *Diabetes.* 50:77–82. https://doi.org/10.2337/diabetes.50.1.77

Boutin, C., and L. Kodjabachian. 2019. Biology of multiciliated cells. *Curr. Opin.Genet. Dev.* 56:1–7. https://doi.org/10.1016/j.gde.2019.04.006

Brooks, E.R., and J.B. Wallingford. 2014. Multiciliated cells. *Curr. Biol.* 24: R973–R982. https://doi.org/10.1016/j.cub.2014.08.047

Bubici, C., and S. Papa. 2014. JNK signalling in cancer: In need of new, smarter therapeutic targets. *Br. J. Pharmacol.* 171:24–37. https://doi.org/10.1111/bph.12432

Burke, M.C., F.Q. Li, B. Cyge, T. Arashiro, H.M. Brechbuhl, X. Chen, S.S. Siller, M.A. Weiss, C.B. O'Connell, D. Love, et al. 2014. Chibby promotes ciliary vesicle formation and basal body docking during airway cell differentiation. *J. Cell Biol.* 207:123–137. https://doi.org/10.1083/jcb.201406140

Čajánek, L., and E.A. Nigg. 2014. Cep164 triggers ciliogenesis by recruiting Tau tubulin kinase 2 to the mother centriole. *Proc. Natl. Acad. Sci. USA.* 111:E2841–E2850. https://doi.org/10.1073/pnas.1401777111

Chatzifrangkeskou, M., and P.A. Skourides. 2022. The apical ciliary adhesion complex is established at the basal foot of motile cilia and depends on the microtubule network. *Sci. Rep.* 12:19028–19112. https://doi.org/10.1038/s41598-022-22871-0

Chevalier, B., A. Adamiok, O. Mercey, D.R. Revinski, L.E. Zaragosi, A. Pasini, L. Kodjabachian, P. Barbry, and B. Marcet. 2015. miR-34/449 control apical actin network formation during multiciliogenesis through small GTPase pathways. *Nat. Commun.* 6:8386–8414. https://doi.org/10.1038/ncomms9386

Chih, B., P. Liu, Y. Chinn, C. Chalouni, L.G. Komuves, P.E. Hass, W. Sandoval, and A.S. Peterson. 2011. A ciliopathy complex at the transition zone protects the cilia as a privileged membrane domain. *Nat. Cell Biol.* 14: 61–72. https://doi.org/10.1038/ncb2410

Christerson, L.B., C.A. Vanderbilt, and M.H. Cobb. 1999. MEKK1 interacts with-actinin and localizes to stress fibers and focal adhesions. *Cell Motil.*

Cytoskeleton. 43:186–198. https://doi.org/10.1002/(SICI)1097-0169(1999)43:3<186::AID-CM2>3.0.CO;2-1

Dawe, H.R., H. Farr, and K. Gull. 2007. Centriole/basal body morphogenesis and migration during ciliogenesis in animal cells. *J. Cell Sci.* 120:7–15. https://doi.org/10.1242/jcs.03305

Derrick, C.J., A. Santos-Ledo, A. Eley, I.A. Paramita, D.J. Henderson, and B. Chaudhry. 2022. Sequential action of JNK genes establishes the embryonic left-right axis. *Development.* 149:dev200136. https://doi.org/10.1242/dev.200136

Drummond, I.A. 2012. Cilia functions in development. *Curr. Opin. Cell Biol.* 24:24–30. https://doi.org/10.1016/j.ceb.2011.12.007

Dupont, M.A., C. Humbert, C. Huber, Q. Siour, I.C. Guerrera, V. Jung, A. Christensen, A. Pouliet, M. Garfa-Traoré, P. Nitschké, et al. 2019. Human IFT52 mutations uncover a novel role for the protein in microtubule dynamics and centrosome cohesion. *Hum. Mol. Genet.* 28:2720–2737. https://doi.org/10.1093/hmg/ddz091

Egorova, A.D., P.P. Khedoe, M.J. Goumans, B.K. Yoder, S.M. Nauli, P. ten Dijke, R.E. Poelmann, and B.P. Hierck. 2011. Lack of primary cilia primes shear-induced endothelial-to-mesenchymal transition. *Circ. Res.* 108:1093–1101. https://doi.org/10.1161/CIRCRESAHA.110.231860

Epting, D., K. Slanchev, C. Boehlke, S. Hoff, N.T. Loges, T. Yasunaga, L. Indorf, S. Nestel, S.S. Lienkamp, H. Omran, et al. 2015. The Rac1 regulator ELMO controls basal body migration and docking in multiciliated cells through interaction with Ezrin. *Development.* 142:174–184. https://doi.org/10.1242/dev.112250

Eyers, C.E., H. McNeill, A. Knebel, N. Morrice, S.J. Arthur, A. Cuenda, and P. Cohen. 2005. The phosphorylation of CapZ-interacting protein (CapZIP) by stress-activated protein kinases triggers its dissociation from CapZ. *Biochem. J.* 389:127–135. https://doi.org/10.1042/BJ20050387

Fosbrink, M., N.N. Aye-Han, R. Cheong, A. Levchenko, and J. Zhang. 2010. Visualization of JNK activity dynamics with a genetically encoded fluorescent biosensor. *Proc. Natl. Acad. Sci. USA.* 107:5459. https://doi.org/10.1073/pnas.0909671107

Gao, Q., J. Zhang, X. Wang, Y. Liu, R. He, X. Liu, F. Wang, J. Feng, D. Yang, Z. Wang, et al. 2017. The signalling receptor MCAM coordinates apical-basal polarity and planar cell polarity during morphogenesis. *Nat. Commun.* 8:15279. https://doi.org/10.1038/ncomms15279

Garcia-Gonzalo, F.R., K.C. Corbit, M.S. Sirerol-Piquer, G. Ramaswami, E.A. Otto, T.R. Noriega, A.D. Seol, J.F. Robinson, C.L. Bennett, D.J. Josifova, et al. 2011. A transition zone complex regulates mammalian ciliogenesis and ciliary membrane composition. *Nat. Genet.* 43:776–784. https://doi.org/10.1038/ng.891

Gonçalves, J., and L. Pelletier. 2017. The ciliary transition zone: Finding the pieces and assembling the gate. *Mol. Cells.* 40:243–253. https://doi.org/10.14348/molcells.2017.0054

Gordon, E.A., T.C. Whisenant, M. Zeller, R.M. Kaake, W.M. Gordon, P. Krotee, V. Patel, L. Huang, P. Baldi, and L. Bardwell. 2013. Combining docking site and phosphosite predictions to find new substrates: Identification of smoothelin-like-2 (SMTNL2) as a c-Jun N-terminal kinase (JNK) substrate. *Cell. Signal.* 25:2518–2529. https://doi.org/10.1016/j.cellsig.2013.08.004

Graser, S., Y.D. Stierhof, S.B. Lavoie, O.S. Gassner, S. Lamla, M. Le Clech, and E.A. Nigg. 2007. Cep164, a novel centriole appendage protein required for primary cilium formation. *J. Cell Biol.* 179:321–330. https://doi.org/10.1083/jcb.200707181

Grynberg, K., F.Y. Ma, and D.J. Nikolic-Paterson. 2017. The JNK signaling pathway in renal fibrosis. *Front. Physiol.* 8:829. https://doi.org/10.3389/fphys.2017.00829

Harding, T.C., L. Xue, A. Bienemann, D. Haywood, M. Dickens, A.M. Tolkovsky, and J.B. Uney. 2001. Inhibition of JNK by overexpression of the JNL binding domain of JIP-1 prevents apoptosis in sympathetic neurons. *J. Biol. Chem.* 276:4531–4534. https://doi.org/10.1074/jbc.C000815200

Hayes, J.M., S.K. Kim, P.B. Abitua, T.J. Park, E.R. Herrington, A. Kitayama, M.W. Grow, N. Ueno, and J.B. Wallingford. 2007. Identification of novel ciliogenesis factors using a new in vivo model for mucociliary epithelial development. *Dev. Biol.* 312:115–130. https://doi.org/10.1016/j.ydbio.2007.09.031

Heo, Y.S., S.K. Kim, C.I. Seo, Y.K. Kim, B.J. Sung, H.S. Lee, J.I. Lee, S.Y. Park, J.H. Kim, K.Y. Hwang, et al. 2004. Structural basis for the selective inhibition of JNK1 by the scaffolding protein JIP1 and SP600125. *EMBO J.* 23:2185–2195. https://doi.org/10.1038/sj.emboj.7600212

Homsy, J.G., H. Jasper, X.G. Peralta, H. Wu, D.P. Kiehart, and D. Bohmann. 2006. JNK signaling coordinates integrin and actin functions during Drosophila embryogenesis. *Dev. Dyn.* 235:427–434. https://doi.org/10.1002/dvdy.20649

Hu, Q., L. Milenkovic, H. Jin, M.P. Scott, M.V. Nachury, E.T. Spiliotis, and W.J. Nelson. 2010. A septin diffusion barrier at the base of the primary cilium maintains ciliary membrane protein distribution. *Science.* 329:436–439. https://doi.org/10.1126/science.1191054

Huang, T., Y. You, M.S. Spoor, E.J. Richer, V.V. Kudva, R.C. Paige, M.P. Seiler, J.M. Liebler, J. Zabner, C.G. Plopper, and S.L. Brody. 2003. Foxj1 is required for apical localization of ezrin in airway epithelial cells. *J. Cell Sci.* 116:4935–4945. https://doi.org/10.1242/jcs.00830

Hyland, R.M., and S.L. Brody. 2021. Impact of motile ciliopathies on human development and clinical consequences in the newborn. *Cells.* 11:125. https://doi.org/10.3390/cells11010125

Ioannou, A., N. Santama, and P.A. Skourides. 2013. Xenopus laevis nucleotide binding protein 1 (xNubp1) is important for convergent extension movements and controls ciliogenesis via regulation of the actin cytoskeleton. *Dev. Biol.* 380:243–258. https://doi.org/10.1016/j.ydbio.2013.05.004

Ishikawa, Y., M. Okada, A. Honda, Y. Ito, A. Tamada, N. Endo, and M. Igarashi. 2019. Phosphorylation sites of microtubule-associated protein 1B (MAP 1B) are involved in axon growth and regeneration. *Mole. Brain.* 12:1–14. https://doi.org/10.1186/s13041-019-0510-z

Joo, K., C.G. Kim, M.S. Lee, H.Y. Moon, S.H. Lee, M.J. Kim, H.S. Kweon, W.Y. Park, C.H. Kim, J.G. Gleeson, and J. Kim. 2013. CCDC41 is required for ciliary vesicle docking to the mother centriole. *Proc. Natl. Acad. Sci. USA.* 110:5987–5992. https://doi.org/10.1073/pnas.1220927110

Kardash, E., J. Bandemer, and E. Raz. 2011. Imaging protein activity in live embryos using fluorescence resonance energy transfer biosensors. *Nat. Protoc.* 6:1835–1846. https://doi.org/10.1038/nprot.2011.395

Komulainen, E., J. Zdrojewska, E. Freemantle, H. Mohammad, N. Kulesskaya, P. Deshpande, F. Marchisella, R. Mysore, P. Hollos, K.A. Michelsen, et al. 2014. JNK1 controls dendritic field size in L2/3 and L5 of the motor cortex, constrains soma size, and influences fine motor coordination. *Front. Cell. Neurosci.* 8:272. https://doi.org/10.3389/fncel.2014.00272

Kulkarni, S.S., J.N. Griffin, P.P. Date, K.F. Liem Jr., and M.K. Khokha. 2018. WDR5 stabilizes actin architecture to promote multiciliated cell formation. *Dev. Cell.* 46:595–610.e3. https://doi.org/10.1016/j.devcel.2018.08.009

Kyriakis, J.M., and J. Avruch. 2001. Mammalian mitogen-activated protein kinase signal transduction pathways activated by stress and inflammation. *Physiol. Rev.* 81:807–869. https://doi.org/10.1152/physrev.2001.81.2.807

Lemullois, M., E. Boisvieux-Ulrich, M.C. Laine, B. Chailley, and D. Sandoz. 1988. Development and functions of the cytoskeleton during ciliogenesis in metazoa. *Biol. Cell.* 63:195–208. https://doi.org/10.1016/0248-4900(88)90058-5

Liao, G., Q. Tao, M. Kofron, J.S. Chen, A. Schloemer, R.J. Davis, J.C. Hsieh, C. Wylie, J. Heasman, and C.Y. Kuan. 2006. Jun NH2-terminal kinase (JNK) prevents nuclear β-catenin accumulation and regulates axis formation in Xenopus embryos. *Proc. Natl. Acad. Sci. USA.* 103:16313–16318. https://doi.org/10.1073/pnas.0602557103

Lv, B., L. Wan, M. Taschner, X. Cheng, E. Lorentzen, and K. Huang. 2017. Intraflagellar transport protein IFT52 recruits IFT46 to the basal body and flagella. *J. Cell Sci.* 130:1662–1674. https://doi.org/10.1242/jcs.200758

Ma, M. 2021. Cilia and polycystic kidney disease. *Semin. Cell Dev. Biol.* 110:139–148. https://doi.org/10.1016/j.semcdb.2020.05.003

Mengistu, M., H. Brotzman, S. Ghadiali, and L. Lowe-Krentz. 2011. Fluid shear stress-induced JNK activity leads to actin remodeling for cell alignment. *J. Cell. Physiol.* 226:110–121. https://doi.org/10.1002/jcp.22311

Mitchell, B., R. Jacobs, J. Li, S. Chien, and C. Kintner. 2007. A positive feedback mechanism governs the polarity and motion of motile cilia. *Nature.* 447:97–101. https://doi.org/10.1038/nature05771

Morton, S., R.J. Davis, A. McLaren, and P. Cohen. 2003. A reinvestigation of the multisite phosphorylation of the transcription factor c-Jun. *EMBO J.* 22:3876–3886. https://doi.org/10.1093/emboj/cdg388

Naydenov, N.G., A.M. Hopkins, and A.I. Ivanov. 2009. c-Jun N-terminal kinase mediates disassembly of apical junctions in model intestinal epithelia. *Cell Cycle.* 8:2110–2121. https://doi.org/10.4161/cc.8.13.8928

Nommick, A., C. Boutin, O. Rosnet, C. Schirmer, E. Bazellières, V. Thomé, E. Loiseau, A. Viallat, and L. Kodjabachian. 2022. Lrrcc1 and Ccdc61 are conserved effectors of multiciliated cell function. *J. Cell Sci.* 135. https://doi.org/10.1242/jcs.258960

Park, T.J., B.J. Mitchell, P.B. Abitua, C. Kintner, and J.B. Wallingford. 2008. Dishevelled controls apical docking and planar polarization of basal bodies in ciliated epithelial cells. *Nat. Genet.* 40:871–879. https://doi.org/10.1038/ng.104

Pedersen, L.B., I.R. Veland, J.M. Schrøder, and S.T. Christensen. 2008. Assembly of primary cilia. *Dev. Dyn.* 237:1993–2006. https://doi.org/10.1002/dvdy.21521

Popmihajlov, Z., D.J. Sutherland, G.S. Horan, A. Ghosh, D.A. Lynch, P.W. Noble, L. Richeldi, T.F. Reiss, and S. Greenberg. 2022. CC-90001, a c-Jun N-terminal kinase (JNK) inhibitor, in patients with pulmonary fibrosis: Design of a phase 2, randomised, placebo-controlled trial. *BMJ Open Respir. Res.* 9:e001060. https://doi.org/10.1136/bmjresp-2021-001060

Ramkumar, A., B.Y. Jong, and K.M. Ori-McKenney. 2018. ReMAPping the microtubule landscape: How phosphorylation dictates the activities of microtubule-associated proteins. *Dev. Dyn.* 247:138–155. https://doi.org/10.1002/dvdy.24599

Reiter, J.F., O.E. Blacque, and M.R. Leroux. 2012. The base of the cilium: Roles for transition fibres and the transition zone in ciliary formation, maintenance and compartmentalization. *EMBO Rep.* 13:608–618. https://doi.org/10.1038/embor.2012.73

Sang, L., J.J. Miller, K.C. Corbit, R.H. Giles, M.J. Brauer, E.A. Otto, L.M. Baye, X. Wen, S.J. Scales, M. Kwong, et al. 2011. Mapping the NPHP-JBTS-MKS protein network reveals ciliopathy disease genes and pathways. *Cell. Cell.* 145:513–528. https://doi.org/10.1016/j.cell.2011.04.019

Schmidt, K.N., S. Kuhns, A. Neuner, B. Hub, H. Zentgraf, and G. Pereira. 2012. Cep164 mediates vesicular docking to the mother centriole during early steps of ciliogenesis. *J. Cell Biol.* 199:1083–1101. https://doi.org/10.1083/jcb.201202126

Schouteden, C., D. Serwas, M. Palfy, and A. Dammermann. 2015. The ciliary transition zone functions in cell adhesion but is dispensable for axoneme assembly in C. elegans. *J. Cell Biol.* 210:35–44. https://doi.org/10.1083/jcb.201501013

Sedzinski, J., E. Hannezo, F. Tu, M. Biro, and J.B. Wallingford. 2016. Emergence of an apical epithelial cell surface in vivo. *Dev. Cell*. 36:24–35. https://doi.org/10.1016/j.devcel.2015.12.013

Sedzinski, J., E. Hannezo, F. Tu, M. Biro, and J.B. Wallingford. 2017. RhoA regulates actin network dynamics during apical surface emergence in multiciliated epithelial cells. *J. Cell Sci.* 130:420–428. https://doi.org/10.1242/jcs.194704

Sillibourne, J.E., C.G. Specht, I. Izeddin, I. Hurbain, P. Tran, A. Triller, X. Darzacq, M. Dahan, and M. Bornens. 2011. Assessing the localization of centrosomal proteins by PALM/STORM nanoscopy. *Cytoskeleton*. 68:619–627. https://doi.org/10.1002/cm.20536

Slee, J.B., and L.J. Lowe-Krentz. 2013. Actin realignment and cofilin regulation are essential for barrier integrity during shear stress. *J. Cell Biochem.* 114:782–795. https://doi.org/10.1002/jcb.24416

Smith, A.O., J.A. Jonassen, K.M. Preval, R.J. Davis, and G.J. Pazour. 2021. c-Jun N-terminal kinase (JNK) signaling contributes to cystic burden in polycystic kidney disease. *PLoS Genet.* 17:e1009711. https://doi.org/10.1371/journal.pgen.1009711

Solas, M., S. Vela, C. Smerdou, E. Martisova, I. Martínez-Valbuena, M.R. Luquin, and M.J. Ramírez. 2023. JNK activation in Alzheimer's disease is driven by amyloid β and is associated with tau pathology. *ACS Chem. Neurosci.* 14:1524–1534. https://doi.org/10.1021/acschemneuro.3c00093

Spassky, N., and A. Meunier. 2017. The development and functions of multiciliated epithelia. *Nat. Rev. Mol. Cell Biol.* 18:423–436. https://doi.org/10.1038/nrm.2017.21

Stebbins, J.L., S.K. De, T. Machleidt, B. Becattini, J. Vazquez, C. Kuntzen, L.H. Chen, J.F. Cellitti, M. Riel-Mehan, A. Emdadi. et al. 2008. Identification of a new JNK inhibitor targeting the JNK-JIP interaction site. *Proc. Natl. Acad. Sci. USA*. 105:16809–16813. https://doi.org/10.1073/pnas.0805677105

Stephan, A., S. Vaughan, M.K. Shaw, K. Gull, and P.G. McKean. 2007. An essential quality control mechanism at the eukaryotic basal body prior to intraflagellar transport. *Traffic*. 8:1323–1330. https://doi.org/10.1111/j.1600-0854.2007.00611.x

Tanos, B.E., H.J. Yang, R. Soni, W.J. Wang, F.P. Macaluso, J.M. Asara, and M.F. Tsou. 2013. Centriole distal appendages promote membrane docking, leading to cilia initiation. *Genes Dev.* 27:163–168. https://doi.org/10.1101/gad.207043.112

Taschner, M., F. Kotsis, P. Braeuer, E.W. Kuehn, and E. Lorentzen. 2014. Crystal structures of IFT70/52 and IFT52/46 provide insight into intraflagellar transport B core complex assembly. *J. Cell Biol.* 207:269–282. https://doi.org/10.1083/jcb.201408002

Tateishi, K., Y. Yamazaki, T. Nishida, S. Watanabe, K. Kunimoto, H. Ishikawa, and S. Tsukita. 2013. Two appendages homologous between basal bodies and centrioles are formed using distinct Odf2 domains. *J. Cell Biol.* 203:417–425. https://doi.org/10.1083/jcb.201303071

Tony Yang, T., J. Su, W.-J. Wang, B. Craige, G.B. Witman, M.-F. Bryan Tsou, and J.-C. Liao. 2015. Superresolution pattern recognition reveals the architectural map of the ciliary transition zone. *Sci. Rep.* 5:14096. https://doi.org/10.1038/srep14096

Tournier, C., A.J. Whitmarsh, J. Cavanagh, T. Barrett, and R.J. Davis. 1997. Mitogen-activated protein kinase kinase 7 is an activator of the c-jun nh2-terminal kinase. *Proc. Natl. Acad. Sci. USA*. 94:7337–7342. https://doi.org/10.1073/pnas.94.14.7337

Tu, F., J. Sedzinski, Y. Ma, E.M. Marcotte, and J.B. Wallingford. 2018. Protein localization screening in vivo reveals novel regulators of multiciliated cell development and function. *J. Cell Sci.* 131:jcs206565. https://doi.org/10.1242/JCS.206565/265430/AM/PROTEIN-LOCALIZATION-SCREENING-IN-VIVO-REVEALS

Vaisse, C., J.F. Reiter, and N.F. Berbari. 2017. Cilia and obesity. *Cold Spring Harb Perspect. Biol.* 9:a028217. https://doi.org/10.1101/cshperspect.a028217

Vladar, E.K., and J.D. Axelrod. 2008. Dishevelled links basal body docking and orientation in ciliated epithelial cells. *Trends Cell Biol.* 18:517–520. https://doi.org/10.1016/j.tcb.2008.08.004

Volta, F., and J.M. Gerdes. 2017. The role of primary cilia in obesity and diabetes. *Ann. N. Y. Acad. Sci.* 1391:71–84. https://doi.org/10.1111/nyas.13216

Walentek, P., I.K. Quigley, D.I. Sun, U.K. Sajjan, C. Kintner, and R.M. Harland. 2016. Ciliary transcription factors and miRNAs precisely regulate Cp110 levels required for ciliary adhesions and ciliogenesis. *Elife*. 5:e17557. https://doi.org/10.7554/eLife.17557

Wallingford, J.B. 2010. Planar cell polarity signaling, cilia and polarized ciliary beating. *Curr. Opin. Cell Biol.* 22:597–604. https://doi.org/10.1016/j.ceb.2010.07.011

Wang, D.X., Y.Q. Pan, B. Liu, and L. Dai. 2018. Cav-1 promotes atherosclerosis by activating JNK-associated signaling. *Biochem. Biophys. Res. Commun.* 503:513–520. https://doi.org/10.1016/j.bbrc.2018.05.036

Wang, W., C. Ma, Z. Mao, and M. Li. 2004. JNK inhibition as a potential strategy in treating Parkinson's disease. *Drug News Perspect.* 17:646–654. https://doi.org/10.1358/dnp.2004.17.10.873916

Wang, Z.M., X.F. Gao, J.J. Zhang, and S.L. Chen. 2021. Primary cilia and atherosclerosis. *Front. Physiol.* 12:44. https://doi.org/10.3389/fphys.2021.640774

Wei, Q., K. Ling, and J. Hu. 2015. The essential roles of transition fibers in the context of cilia. *Curr. Opin. Cell Biol.* 35:98–105. https://doi.org/10.1016/j.ceb.2015.04.015

Werner, M.E., and B.J. Mitchell. 2012. Understanding ciliated epithelia: The power of Xenopus. *Genesis*. 50:176–185. https://doi.org/10.1002/dvg.20824

Williams, C.L., C. Li, K. Kida, P.N. Inglis, S. Mohan, L. Semenec, N.J. Bialas, R.M. Stupay, N. Chen, O.E. Blacque, et al. 2011. MKS and NPHP modules cooperate to establish basal body/transition zone membrane associations and ciliary gate function during ciliogenesis. *J. Cell Biol.* 192:1023–1041. https://doi.org/10.1083/jcb.201012116

Wu, Q., W. Wu, V. Jacevic, T.C.C. Franca, X. Wang, and K. Kuca. 2020. Selective inhibitors for JNK signalling: A potential targeted therapy in cancer. *J. Enzyme Inhib. Med. Chem.* 351:574–583. https://doi.org/10.1080/14756366.2020.1720013

Xiao, Y., Y. Zhou, Z. Xiong, L. Zou, M. Jiang, Z. Luo, S. Wen, W. Liu, S. Liu, and W. Li. 2013. Involvement of JNK in the embryonic development and organogenesis in zebrafish. *Mar. Biotechnol.* 15:716–725. https://doi.org/10.1007/s10126-013-9520-5

Yamanaka, H., T. Moriguchi, N. Masuyama, M. Kusakabe, H. Hanafusa, R. Takada, S. Takada, and E. Nishida. 2002. JNK functions in the non-canonical Wnt pathway to regulate convergent extension movements in vertebrates. *EMBO Rep.* 3:69–75. https://doi.org/10.1093/embo-reports/kvf008

Yan, M., T. Dai, J.C. Deak, J.M. Kyriakis, L.I. Zon, J.R. Woodgett, and D.J. Templeton. 1994. Activation of stress-activated protein kinase by MEKK1 phosphorylation of its activator SEK1. *Nature*. 372:798–800. https://doi.org/10.1038/372798a0

Yang, C., K. Patel, P. Harding, A. Sorokin, and W.F. Glass 2nd. 2007. Regulation of TGF-β1/MAPK-mediated PAI-1 gene expression by the actin cytoskeleton in human mesangial cells. *Exp. Cell Res.* 313:1240–1250. https://doi.org/10.1016/j.yexcr.2007.01.011

Yarza, R., S. Vela, M. Solas, and M.J. Ramirez. 2016. c-Jun N-terminal kinase (JNK) signaling as a therapeutic target for alzheimer's disease. *Front. Pharmacol.* 6:321. https://doi.org/10.3389/fphar.2015.00321

Yasunaga, T., J. Wiegel, M.D. Bergen, M. Helmstädter, D. Epting, A. Paolini, Ö. Çiçek, G. Radziwill, C. Engel, T. Brox, et al. 2022. Microridge-like structures anchor motile cilia,. *Nat. Commun.* 13:2056–2114. https://doi.org/10.1038/s41467-022-29741-3

Ye, X., H. Zeng, G. Ning, J.F. Reiter, and A. Liu. 2014. C2cd3 is critical for centriolar distal appendage assembly and ciliary vesicle docking in

mammals. *Proc. Natl. Acad. Sci. USA*. 111:2164–2169. https://doi.org/10.1073/pnas.1318737111

Yung, J.H.M., and A. Giacca. 2020. Role of c-Jun N-terminal kinase (JNK) in obesity and type 2 diabetes. *Cells*. 9:706. https://doi.org/10.3390/cells9030706

Zhang, S., and B.J. Mitchell. 2015. Centriole biogenesis and function in multiciliated cells. *Methods Cell Biol.* 129:103–127. https://doi.org/10.1016/bs.mcb.2015.03.015

Zhang, W., S.P. Taylor, L. Nevarez, R.S. Lachman, D.A. Nickerson, M. Bamshad, University of Washington Center for Mendelian Genomics Consortium, D. Krakow, D.H. Cohn, et al. 2016. IFT52 mutations destabilize anterograde complex assembly, disrupt ciliogenesis and result in short rib polydactyly syndrome. *Hum. Mol. Genet.* 25:4012. https://doi.org/10.1093/hmg/ddw241

Zhang, W., S.P. Taylor, H.A. Ennis, K.N. Forlenza, I. Duran, B. Li, J.A.O. Sanchez, L. Nevarez, D.A. Nickerson, M. Bamshad, et al. 2018. Expanding the genetic architecture and phenotypic spectrum in the skeletal ciliopathies. *Hum. Mutat.* 39:152–166. https://doi.org/10.1002/humu.23362
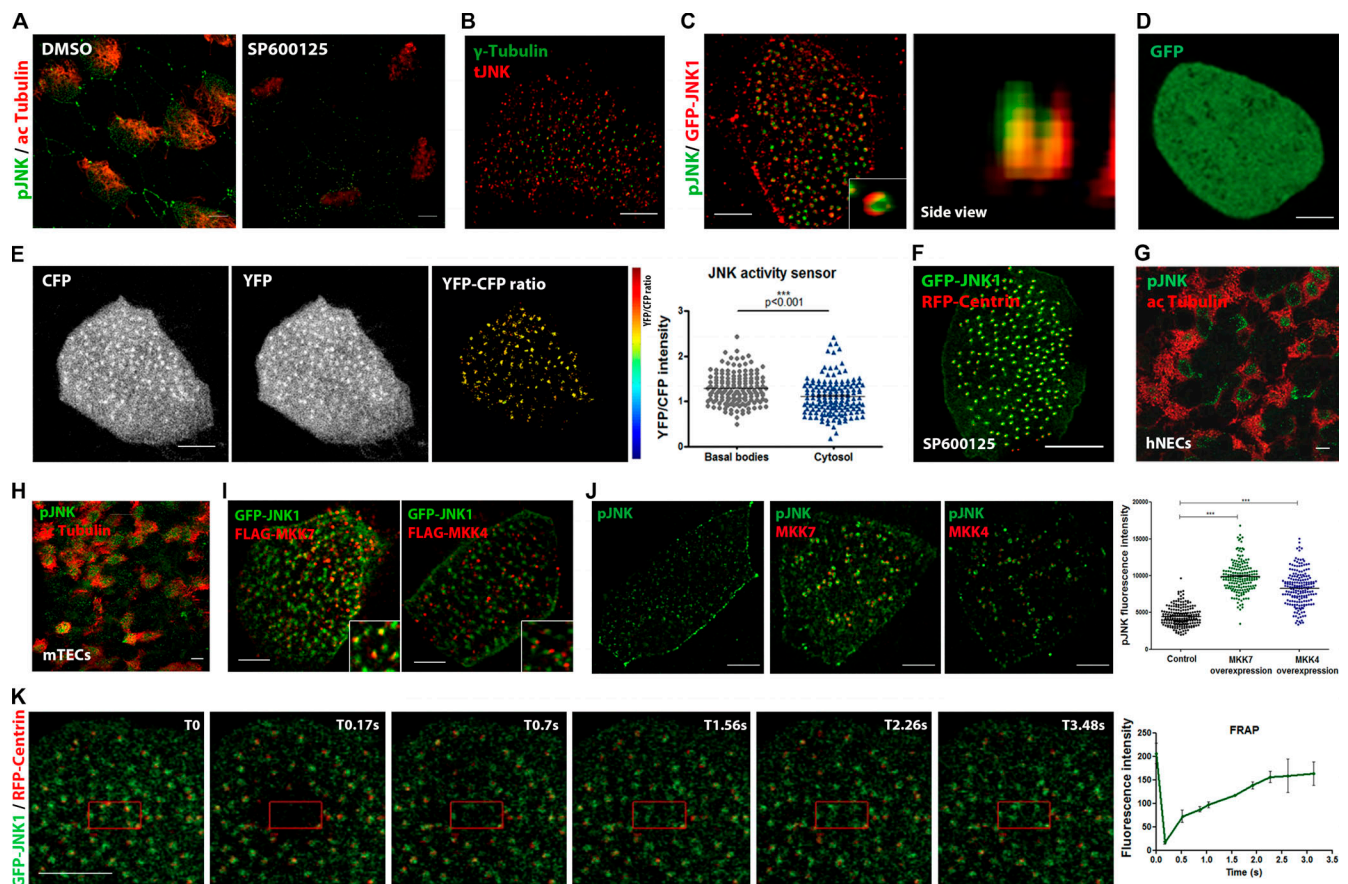
Figure S1. **Active JNK is localized at the base of motile cilia. (A)** Immunofluorescence images of DMSO- and SP600125-treated embryos stained with pJNK and acetylated tubulin to mark MCCs. Scale bars, 5 μm. **(B)** Multiciliated cells stained for total JNK (tJNK) and γ-tubulin that marks the basal foot. **(C)** Multiciliated cells expressing GFP-JNK stained with an antibody against pJNK. Side view (XZ projection) shows an overlap of the two signals. Scale bars, 10 μm. **(D)** Confocal images of *Xenopus* epidermal MCCs injected with GFP displaying a diffuse cytosolic pattern. Scale bars, 10 μm. **(E)** Color-coded images of the YFP/CFP intensity ratio of the JNK biosensor showing higher ratio at the basal bodies. Graph shows the quantification of the YFP to CFP intensity ratio of the JNK FRET sensor at the basal bodies and cytosol. YFP/CFP ratio at the BBs is higher than in the cytosol. Data represent ± SEM from two experiments (n = 159 BBs, and n = 156 cytosolic regions from 4 embryos), ***, P < 0.001, unpaired two-tailed *t* test. Scale bars, 5 μm. **(F)** Representative confocal images of SP600125-treated embryos injected with GFP-JNK and RFP-Centrin. JNK localization is not dependent on its kinase activity. Scale bars, 5 μm. **(G)** Representative images of human nasal epithelial cells (hNECs) grown at ALI after 21–25 d. Staining with acetylated tubulin and pJNK show apical enrichment of pJNK. Scale bars, 5 μm. **(H)** Representative confocal images of endogenous localization of acetylated tubulin and pJNK in mouse tracheal epithelial cells (mTECs). Scale bars, 5 μm. **(I)** Confocal images of MCCs expressing GFP-JNK coinjected with FLAG-MKK7 show partial colocalization with JNK. Expression of FLAG-MKK4 show apical enrichment. Scale bars, 5 μm. **(J)** Representative images of pJNK staining in Flag-MKK7 and Flag-MKK4 overexpressing MCCs. Quantification of BB-associated fluorescence signal of pJNK shows enhanced phosphorylation in MKK7- and MKK4-overexpressing cells compared to controls (n = 205 controls, n = 179 MKK7-overexpressing cells, n = 192 MKK4-overexpressing cells). Data represent ± SEM from three experiments. ***, P < 0.001, unpaired two-tailed *t* test. **(K)** Image sequence of a MCC expressing GFP-JNK/RFP-Centrin upon photobleaching of a region of interest (red square). T0 indicates the time of photobleaching. Normalized fluorescence intensity of GFP-JNK displays a highly dynamic association of JNK with the basal bodies with t1/2 = 0.4 s (n = 11 controls and n = 11 JNK MO from 3 embryos). Scale bars, 10 μm.
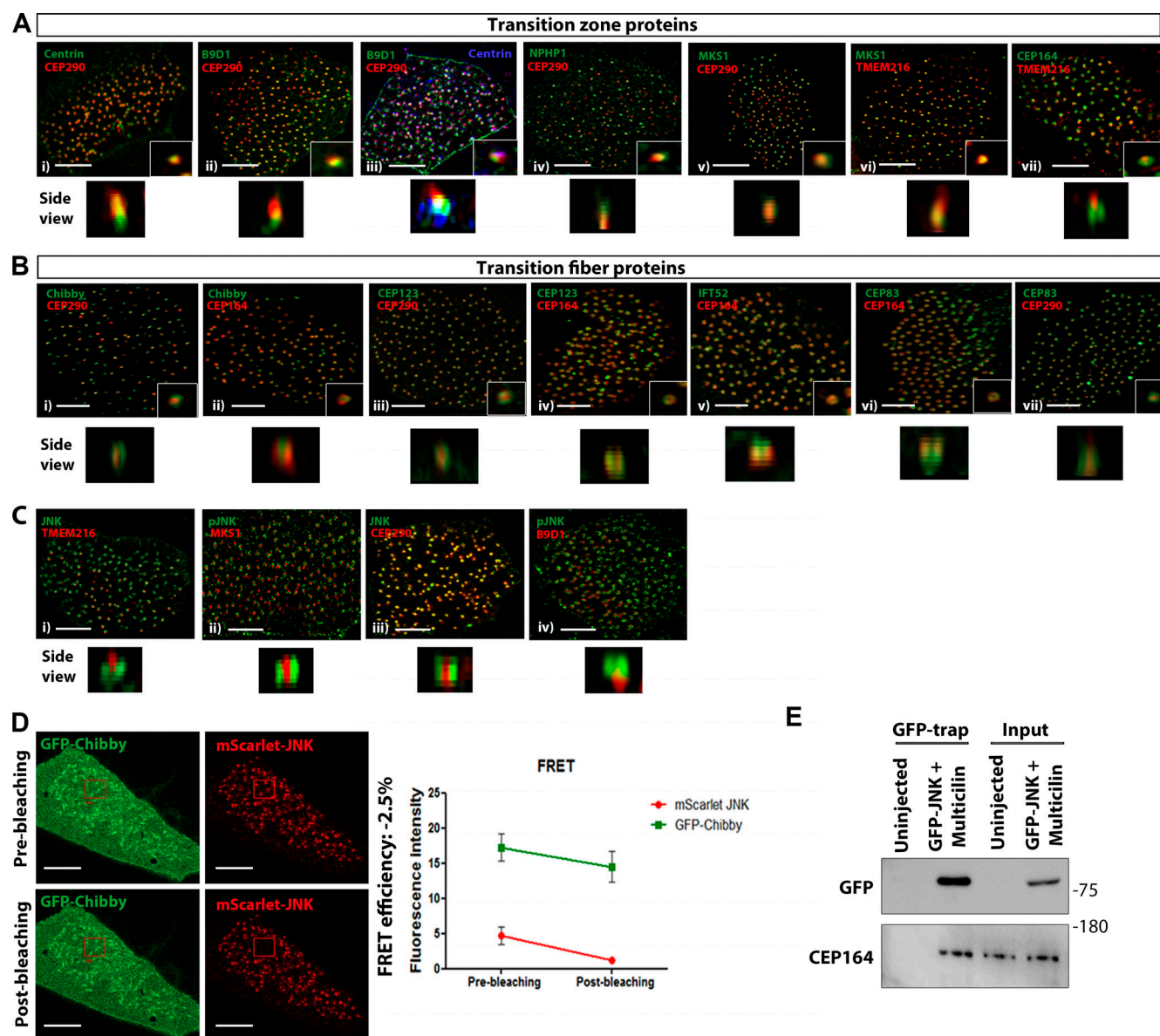
Figure S2. **Map of TZ and TF components of epidermal motile cilia. (A)** Airyscan super-resolution Z-stack images of MCCs expressing the transition zone proteins (i) mTagBFP2-Centrin and mCherry-CEP290, (ii) mEmerald-B9D1 and mCherry-CEP290, (iii) mTagBFP2-Centrin, mEmerald-B9D1 and mCherry-CEP290, (iv) mEmerald-NPHP1 and mCherry-CEP290, (v) mEmerald-MKS1 and mCherry-CEP290, (vi) mEmerald-MKS1 and mCherry-TMEM216, and (vii) mCherry-TMEM216 and stained for CEP164. Scale bars, 5 µm. **(B)** Representative Z-stack images of MCCs expressing the transition fiber proteins (i) GFP-Chibby and mCherry-CEP290, (ii) GFP-Chibby stained for CEP164, (iii) GFP-CEP123 and mCherry-CEP290, (iv) GFP-CEP123 stained for CEP164, (v) GFP-IFT52 stained for CEP164, (vi) GFP-CEP83 stained for CEP164, and (vii) GFP-CEP83 and mCherry-CEP290. Scale bars, 5 µm. **(C)** Airyscan super-resolution Z-stack images of MCCs expressing (i) GFP-JNK1 and mCherry-TMEM216, (ii) mEmerald-MKS1 stained for pJNK, (iii) GFP-JNK1 and mCherry-CEP290, and (iv) mEmerald-B9D1 stained for pJNK. Scale bars, 5 µm. **(D)** Multiciliated cell expressing mScarlet JNK (acceptor) and GFP-Chibby. GFP intensity remains unchanged suggesting that JNK is not associated with Chibby. Data represent mean ± SEM (n = 6 MCCs from three embryos). Scale bars, 5 µm. **(E)** Western blot showing that immunoprecipitated GFP-JNK from uninjected and Multicilin overexpressing skin lysates interacts with CEP164. Source data are available for this figure: SourceData FS2.
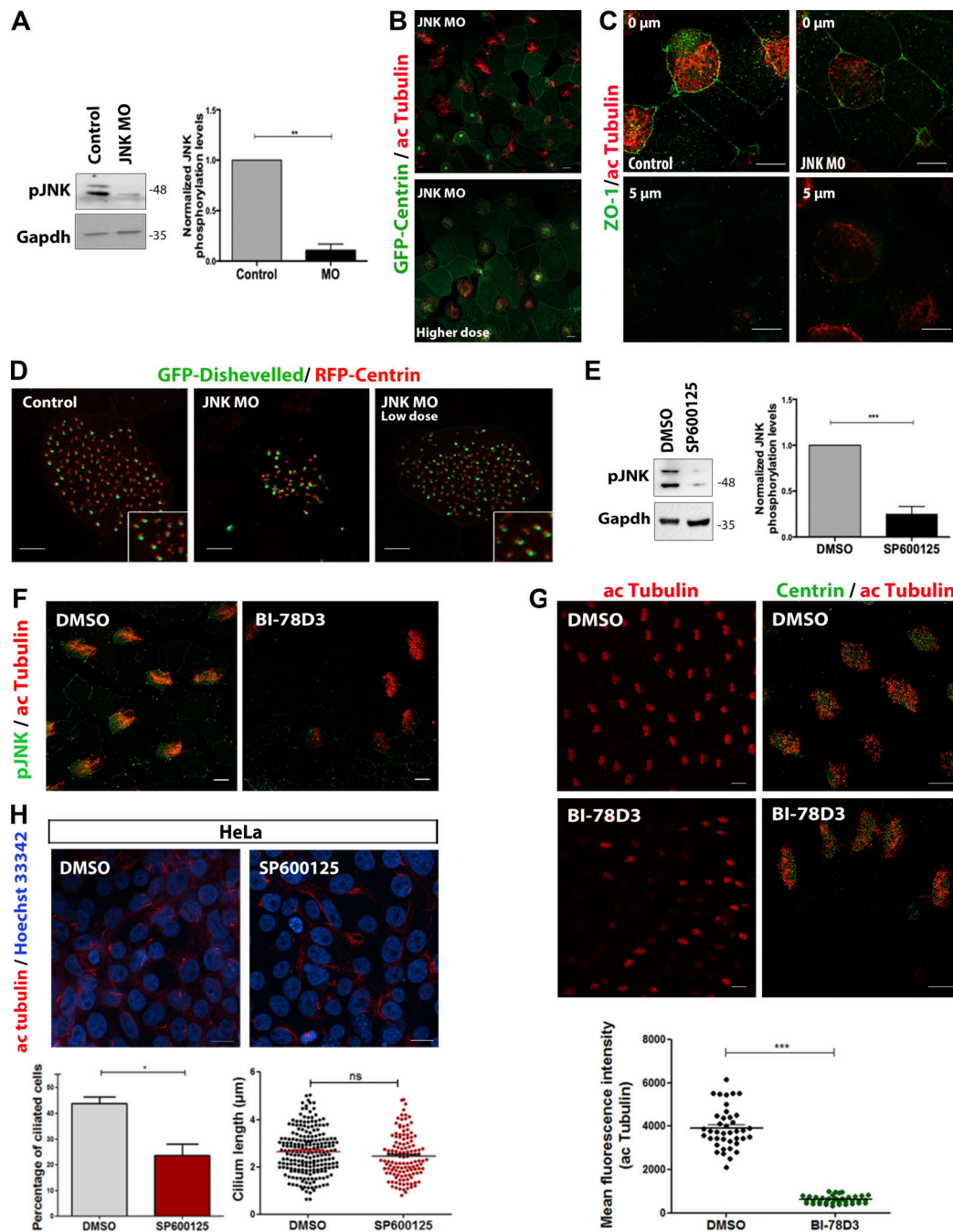
Figure S3.   **Inhibition of JNK activity affects primary and motile ciliogenesis. (A)** Western blot analysis of protein extracts from control and JNK morphants. 40 ng of JNK MO was injected into both blastomeres of two-cell stage embryos. Quantification shows the normalized ratio of pJNK/GAPDH intensity. Data represent mean ± SEM from three independent experiments. **, P < 0.01, unpaired two-tailed *t* test. **(B)** Representative images of GFP-Centrin expressing embryos injected with high dose MO (80 ng/cell) and stained with acetylated tubulin. Scale bars, 5 μm. **(C)** Immunofluorescence images of control and JNK MO embryos stained for acetylated tubulin and ZO-1 shows apical enrichment of ZO-1 and absence of signal at the basal region. Scale bars, 10 μm. **(D)** Representative images of control and JNK MO (low and high dose) embryos injected with GFP-Dishevelled shows an association of Dishevelled with the basal bodies, suggesting that JNK is not involved in the PCP polarity. Scale bars, 5 μm. **(E)** Western blotting of pJNK protein levels in DMSO- or SP600125-treated epidermal lysates. Quantification shows the normalized ratio of pJNK/GAPDH intensity. Data represent mean ± SEM from three independent experiments, ***, P < 0.001, unpaired two-tailed *t* test. **(F)** Immunofluorescence images of DMSO- and BI-78D3 embryos stained for pJNK and acetylated Tubulin. Fluorescence intensity of pJNK in BI-78D3-treated embryos is dramatically decreased compared with DMSO. Scale bars, 5 μm. **(G)** Immunofluorescence images of DMSO- and BI-78D3 embryos stained for Centrin and acetylated tubulin. Scale bars, 10 μm. Quantification shows decreased acetylated-tubulin fluorescence intensity in BI-78D3-treated MCCs compared to DMSO. Data represent mean ± SEM from three independent experiments, ***, P < 0.001, unpaired two-tailed *t* test. **(H)** HeLa cells were serum-starved for 24 h and stained for acetylated α-tubulin in the presence of DMSO or SP600125. DNA was counterstained with Hoechst. Scale bars, 20 μm. Primary cilia were manually counted by scanning through all focal planes. Approximately 700 cells for each condition were scored from three replicates for the presence of a primary cilium. The percentage of primary cilia in SP600125-treated cells is decreased as shown in the graph. Data represent mean ± SEM from three independent experiments, *, P < 0.05, unpaired two-tailed *t* test. Source data are available for this figure: SourceData FS3.
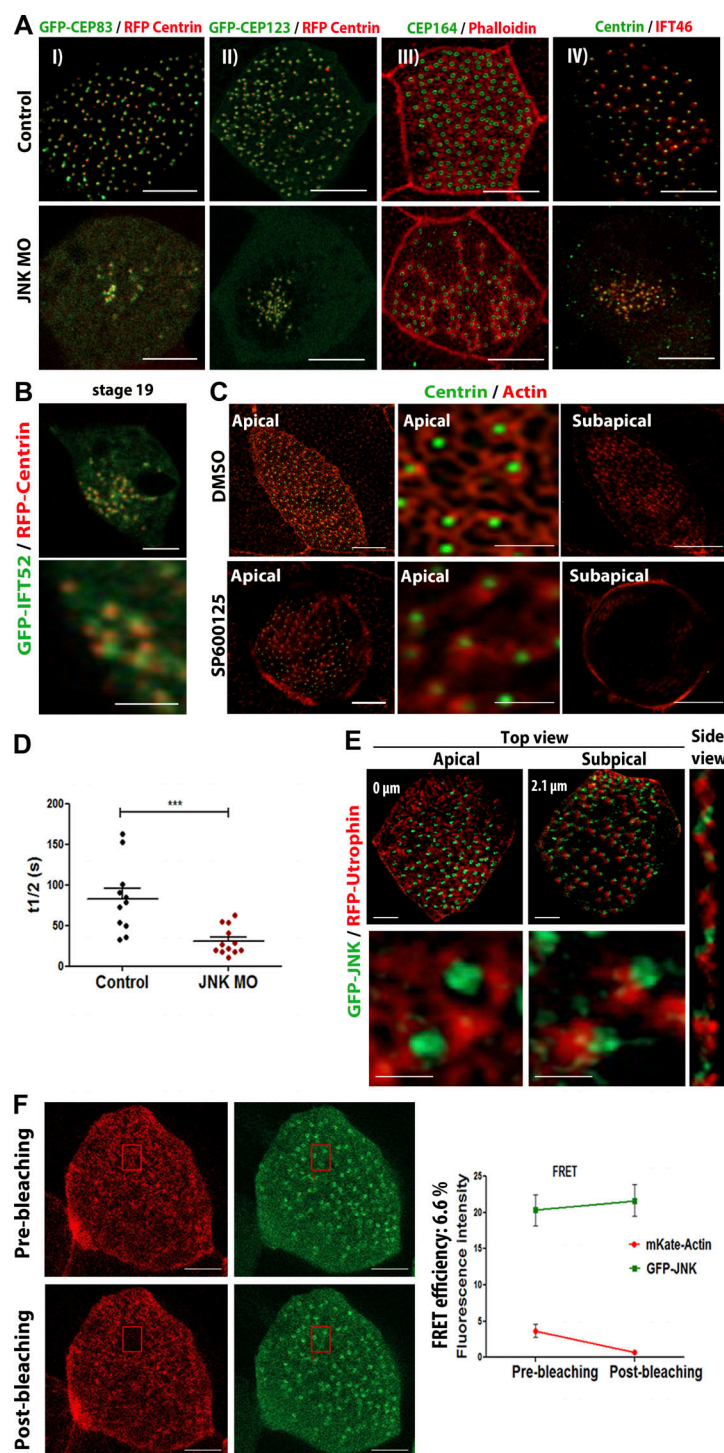
Figure S4. **JNK is involved in the association of IFT-52 with the basal bodies and apical actin network establishment. (A)** (I) Representative images of embryos injected with GFP-CEP83 and RFP-Centrin in control and JNK MO embryos. (II) Images of embryos injected with GFP-CEP123 and RFP-Centrin in control and JNK MO embryos. (III) Control and JNK morphants stained with Phalloidin and CEP164. (IV) Representative image of MCC injected with mCherry-IFT46 and stained for Centrin. The association of CEP83, CEP123, CEP164 and IFT46 with the basal bodies is not affected in JNK morphants. Scale bars, 10 μm. **(B)** Representative confocal images of stage 19 embryos coinjected with GFP-IFT52 and RFP-Centrin. IFT52 is associated with the basal bodies during the early stages of ciliogenesis. Scale bars, 5 μm. **(C)** MCCs of DMSO- and SP600125-treated embryos stained with phalloidin to visualize apical and subapical actin networks. Single optical sections show impaired apical and subapical actin networks in SP600125-treated embryos. Scale bars, 5 μm. **(D)** Quantification of the half-time of recovery (t1/2) of apical actin in control and JNK morphant MCCs. Error bars indicate ± SEM. ***, P < 0.001, unpaired two-tailed t test. **(E)** Optical sections of a *Xenopus* epidermal MCC expressing GFP-JNK and RFP-Utrophin. A second region of JNK enrichment in close association with the subapical actin is occasionally detected. Scale bars, 5 μm. **(F)** Multiciliated cell expressing GFP-JNK (donor) and mKate2 Actin (acceptor) showing the apical actin network, before and after acceptor photobleaching (n = 5 from 3 embryos). GFP intensity rises, showing that FRET is taking place between GFP and mKate2 suggesting that JNK interacts with actin. Scale bars, 10 μm.
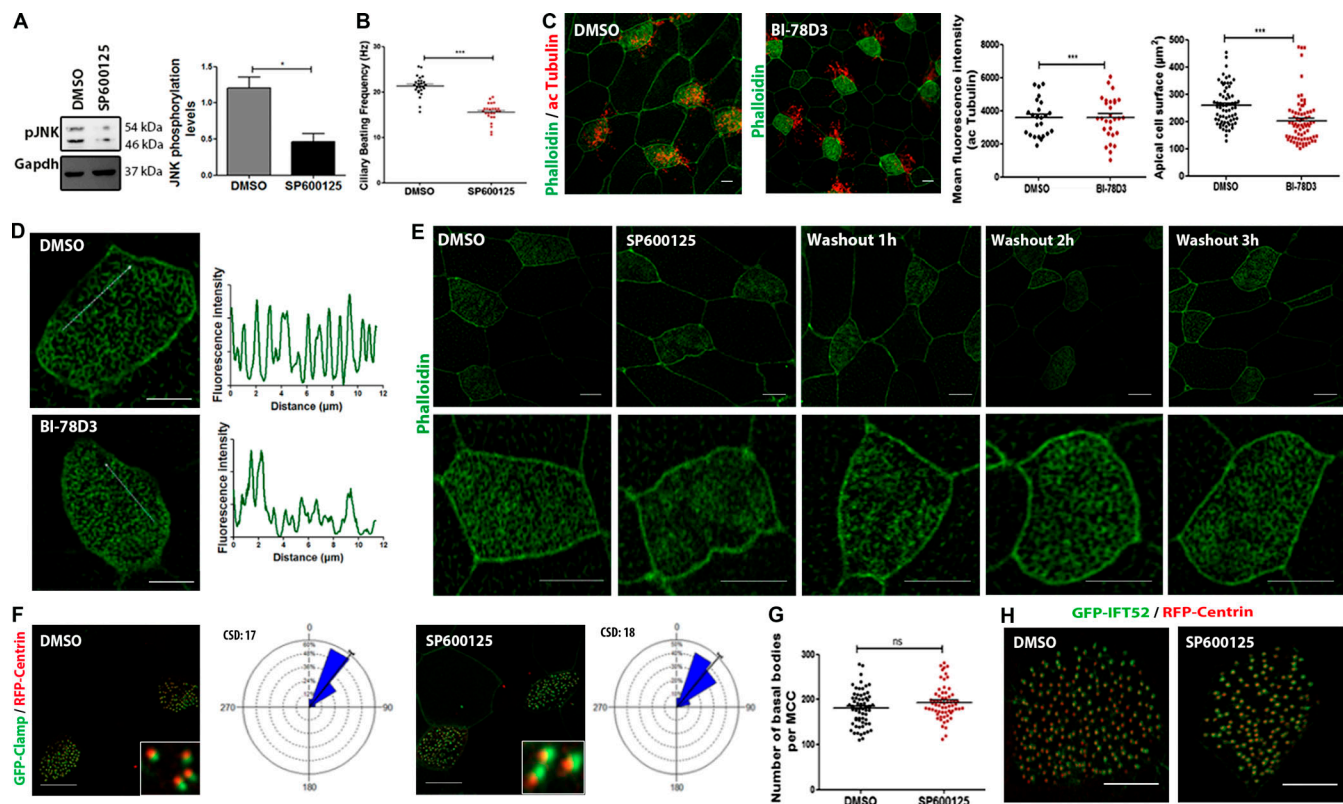
Figure S5. **Inhibition of JNK in mature MCCs leads to defects in CBF and apical actin without affecting rotational polarity. (A)** Western blot analysis of pJNK protein levels in tadpoles' skin lysate from DMSO- or SP600125-treated embryos. *, P < 0.05, data represent mean ± SEM from three independent experiments, unpaired two-tailed *t* test. **(B)** Ciliary beat frequency in hertz (beats per second) of motile cilia in DMSO- or SP600125-treated *Xenopus* epidermal MCCs. Error bars indicate ± SEM, ***, P < 0.001 (*n* = 5 embryos for each condition), unpaired two-tailed *t* test. **(C)** Immunofluorescence images of DMSO- and BI-78D3 embryos labeled for F-actin and acetylated tubulin. Scale bars, 10 μm. Quantification shows decreased acetylated tubulin intensity (*n* = 23 DMSO-treated MCCs and *n* = 28 BI-78D3-treated MCCs) and apical cell surface (*n* = 33 DMSO-treated MCCs, *n* = 57 BI-78D3-treated MCCs) in BI-78D3-treated embryos compared to DMSO. Error bars indicate ± SEM from three experiments, ***, P < 0.001, unpaired two-tailed *t* test. **(D)** Representative higher-magnification immunofluorescence images of MCC treated with DMSO or BI-78D3 for 2 h and stained with Phalloidin. Fluorescence intensity profiles along the lines show an impaired apical actin network in BI-78D3-treated MCCs. Scale bars, 10 μm. **(E)** Immunofluorescence images of MCCs treated with SP600125 for 2 h at stage 30 followed by drug washout and subsequent imaging of the apical actin network 0, 1, 2, and 3 h after washout. Scale bars, 10 μm. **(F)** Representative images of DMSO- and SP600125-treated embryos injected with GFP-Clamp as a marker of rootlets and RFP-Centrin to monitor cilia orientation. Circular diagrams of mean cilia orientation from polarized embryos treated at stage 30 with either DMSO or SP600125 for 2 h (*n* = 212 BB from four DMSO-treated embryos, *n* = 243 BBs from 4 SP600125-treated embryos). Rotational polarity is not affected in SP600125-treated embryos as reflected by the similar circular standard deviation (CSD). Scale bars, 10 μm. **(G)** Quantification of the number of basal bodies in DMSO- (*n* = 63 MCCs from three embryos) and SP60125-treated stage 30 embryos (*n* = 61 from 3 embryos). Error bars indicate ± SEM from two experiments, unpaired two-tailed *t* test. **(H)** Confocal images of stage 30 embryos coinjected with GFP-IFT52 and RFP-Centrin. The association of IFT52 with the basal bodies is not affected in 2 h SP600125-treated embryos. Scale bars, 10 μm. Source data are available for this figure: SourceData FS5.

Chatzifrangkeskou et al.
JNK is involved in ciliogenesis

Journal of Cell Biology S5
https://doi.org/10.1083/jcb.202303052